CHEMOSTRATIGRAPHY OF THE LATE CRETACEOUS EAGLE FORD GROUP, SOUTH TEXAS

by

ROBERT FRANCIS NIKIRK

Presented to the Faculty of the Graduate School of
The University of Texas at Arlington in Partial Fulfillment
of the Requirements
for the Degree of

MASTER OF SCIENCE IN GEOLOGY

THE UNIVERSITY OF TEXAS AT ARLINGTON

May 2014

Acknowledgements

Foremost, I would like to thank my advisor, Dr. Harry Rowe, for his time, energy and patience over the past few years. This thesis would not have been possible without his guidance. I also wish to thank the members of my graduate committee, Dr. John Wickham and Dr. Andrew Hunt, for their counsel and insight, both in class and in conversations.

I would also like to express my gratitude to several members of the Bureau of Economic Geology in Austin, Texas. I would like to thank Dr. Stephen Ruppel for providing core access and material support for this project. In addition I wish to thank James Donnelly, Nathan Ivicic, Kenneth Edwards, and Josh Lambert for their assistance in the access and handling of the studied cores.

I am very grateful for the assistance and counsel of my fellow members of Dr. Rowe's geochemistry research group at the University of Texas at Arlington. I wish to thank Krystin Robinson, Jessica Buckles, James Hoelke, Rolando Castilleja, and Karen McCreight for their support and encouragement these past few years.

Finally, I would like to thank my amazing family for their encouragement and unwavering support in my return to college to earn my degree. I am eternally grateful for your faith in me.

April 18, 2014

Abstract

CHEMOSTRATIGRAPHY OF THE LATE
CRETACEOUS EAGLE FORD GROUP,
SOUTH TEXAS

Robert Nikirk, M.S.

The University of Texas at Arlington, 2014

Supervising Professor: Harold Rowe

Strata of the Eagle Ford Group of South Texas, deposited during the Cenomanian and Turonian of the Late Cretaceous, are largely characterized as mixed siliciclastic and carbonate mudrocks rich in organic carbon. The Eagle Ford Group records deposition within the Maverick Basin, along the Comanche Shelf, at the southern margin of the Western Interior Seaway in present-day South Texas. In recent years, the Eagle Ford has emerged as one of the premiere petroleum plays, as it has been proven to be capable of producing significant volumes of dry gas, wet gas/condensates, and oil. It is believed the Eagle Ford represents deposition during the globally correlative Ocean Anoxic Event #2, characterized by the accumulation and preservation of vast amounts of organic carbon due to the expansion of large deep-water oxygen minimum zones.

This study integrates geochemical analyses of six drill cores from Gonzales, Guadalupe, La Salle and Wilson counties of South Texas. These cores were studied to determine bulk geochemistry, redox conditions, and degree of basin restriction and deep-water renewal times in order to provide a detailed assessment of the chemostratigraphy and paleoceanography of the Eagle Ford Group. Each core was scanned at one foot

intervals with a handheld X-ray fluorescence (XRF) spectrometer to obtain quantitative measurements of major elements, such as Ca, Al and Si, as well as redox sensitive trace metals, such as V, Zn, Ni and Mo. In addition, some cores were analyzed for total organic carbon (TOC), total inorganic carbon (TIC), and stable isotope ($\delta^{13}C$ and $\delta^{18}O$) signatures of the inorganic, carbonate component.

The elevated levels of redox sensitive trace metals of the Lower Eagle Ford, represented here by the Lake Waco and Pepper Shale Formations, reveals deposition during a time of anoxic or euxinic conditions leading to the preservation of large amounts of organic carbon (~5% TOC). The South Bosque Formation, representing the Upper Eagle Ford, displays reduced levels of these trace metals, suggesting a return to a more oxygenated environment prior to the deposition of the overlying, fully oxygenated and heavily bioturbated Austin Chalk. The physical paleoceanography of the Eagle Ford is revealed to be restricted at times and more open at others with lower deep-water renewal times, yet remained mainly within an anoxic or euxinic state. In regard to the inorganic stable isotopic data, the $\delta^{13}C_{carb}$ values, which other studies have shown to display a positive excursion at the time of OAE2, suggest this event is not preserved within the cores analyzed.

Table of Contents

List of Illustrations

List of Tables

Chapter 1

Introduction

1.1 Purpose of Study

The Eagle Ford in South Texas has long been known as source rock for the hydrocarbon reservoirs in the Austin Chalk and Buda Limestone. Newer technologies, such as hydraulic fracturing, have demonstrated that the Eagle Ford can be exploited for significant volumes of dry gas, wet gas/condensate, and oil. Discoveries of producible unconventional petroleum systems in the Barnett, Woodford, Pearsall and Eagle Ford have led to heightened industry focus on these mudrock systems.

Mudrocks make up roughly two-thirds of the sedimentary rock record and contain large portions of earth's stratigraphic history, usually in relatively continuous successions (Blatt, 1980; Potter et al., 1980; Schieber and Zimmerlee, 1998; Aplin et al., 1999). They have been traditionally considered to be monotonous, fine-grained successions that show little lithologic variability. Geochemical analyses of mudrock drill cores can provide valuable scientific information. They may provide insight into depositional environments, paleoceanography, paleoclimate, and information on the burial and preservation of organic matter. These analyses are particularly useful in mudrocks deposited in marine sedimentary basins, as these may serve as source rocks and reservoirs for economically vital hydrocarbon deposits (Arthur and Sageman, 1994; Schieber and Zimmerle, 1998; Aplin et al., 1999; Piper and Calvert, 2009). Previous studies of mudrocks have proven useful in determining paleo-conditions such as degree of basinal restriction, deep water renewal times, redox conditions, and ocean chemistry and circulation (Dean and Arthur, 1989; Calvert and Pedersen, 1993; Piper, 1994; Algeo and Maynard, 2004; Piper and Perkins, 2004; Rimmer, 2004; Algeo et al., 2008; Rowe et al., 2008; Piper and Calvert, 2009; Algeo and Rowe, 2011).

1.2 Geological Information

1.2.1 Geographic Setting

For most of the Late Cretaceous the Western Interior Seaway (WIS) crossed the North American craton, extending from Arctic Canada south to the Gulf of Mexico (Williams and Stelck, 1975; Kauffman, 1977) (Figure 1.1**).** This encroachment of marine waters began with a northern flooding arm in the Aptian. This northern arm met with the southern encroachment arm in southern Colorado in the Albian and remained as a continuous marine system for 35Ma, until the Middle Maastrichtian (Kauffman, 1984). To the east of the WIS lies the broad, stable cratonic platform while to the west lies the Cordilleran thrust belt with volcanic centers in New Mexico-Arizona and Idaho-Montana (Kauffman, 1977).

During this time, at the southern end of the WIS in present day Texas, the Comanche Shelf developed as thick progradational carbonate packages (Fairbanks, 2012). It was along this carbonate shelf, in the Middle to Late Cenomanian, that the Eagle Ford was deposited as a mixed siliciclastic-carbonate mud accumulation during an otherwise carbonate dominated accumulation period (Haq et al., 1987; Mancini et al., 2005; Galloway, 2008). The southern-most expression of the Grenville orogeny is the Paleozoic Llano Uplift (Culotta, et al., 1992). The San Marcos Arch is an extension of the Llano Uplift that trends southeast-northwest. Due to its decreased subsidence, the San Marcos Arch served as a minor topographic high and separated the Maverick Basin from the East Texas Basin.

Figure 1.1 Eagle Ford deposition in Late Cretaceous North America, 92Ma (Turonian).

Modified after Bakey, 2014.

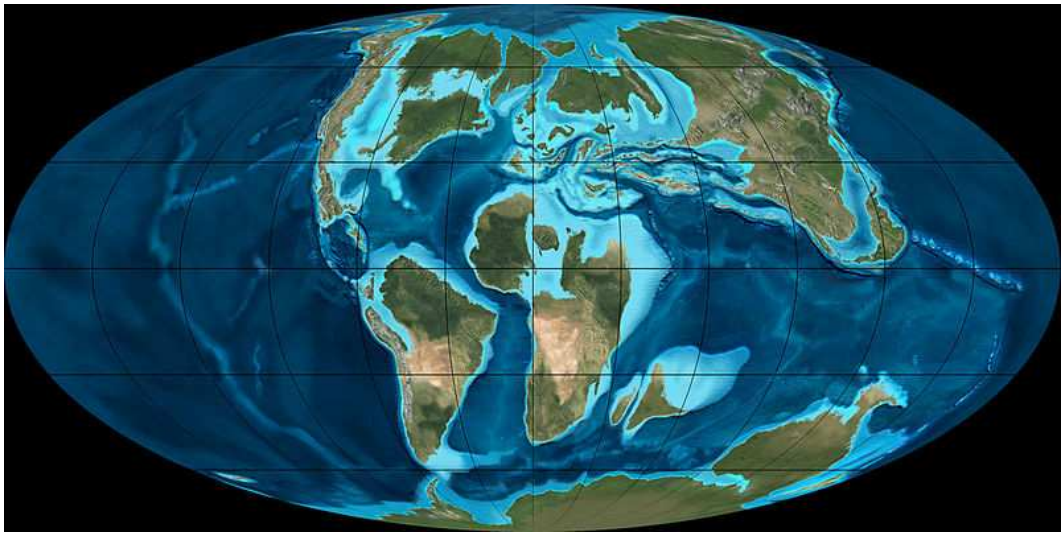

Figure 1.2 Global paleogeographic reconstruction, 95Ma (Cenomanian) (Blakey, 2012).

1.2.2 Paleoclimate

The Cretaceous-age Earth was significantly different from modern conditions on the planet. An increase in global volcanic activity released large amounts of greenhouse gases, such as CO_2, into the atmosphere. This led to an increase in global temperatures and an absence of polar ice and continental glaciers (Barron, 1983; Arthur et al., 1985). It is estimated that the temperature gradient between the equator and polar regions was 35℃ or less, and that tropical temperatures of the Late Cretaceous were between 4 and 14℃ warmer than today (Barron, 1983; Bice et al., 2006). The lack of water locked up in surface ice, coupled with an increase in sea-floor spreading, with the opening of the Atlantic Ocean, resulted in some of the highest recorded sea-levels. Estimations of sea level rise vary between 130 m and 180 m above that of today, with a maximum sea level placed around 200 m higher than today (Harrison, 1990; Vail et al., 1977; Haq et al., 1986; Sahagian et al., 1996). With this eustatic rise, many low lying areas were covered by warm, shallow, organic rich seas and waterways, such as the Western Interior

Seaway (WIS) that crossed western North America linking the Arctic Sea with the Gulf of Mexico for much of the Cretaceous (Mancini and Puckett, 2005). With the break-up of the Pangea supercontinent there existed a continuous equatorial seaway that circulated warm water around the globe (Figure 1.2).

Ocean circulation was markedly different than the global Thermohaline Conveyor we see today, in which the growth of sea ice leaves behind cold, denser than normal water the sinks and is transported along the ocean depths to warmer, lower latitudes, with a compensatory flow of shallow warmer water. The lack of a conveyor such as this resulted in a stalling of the circulation of oxygenated sea water and a stratification of the water column.

Influxes of CO_2 into the atmosphere, leading to a rapid increase in global temperature, melting of the ice caps and lack of circulation of oxygenated sea water are all contributing factors in the expansion of oxygen minimum zones that lead to the occurrence of correlative climatic events, known as ocean anoxic events (OAEs) (Schlanger and Jenkyns, 1976; Jenkyns, 2010). The onset of these events was also aided by an increase in organic productivity, thus depleting the available oxygen. This increase in productivity can by induced by increased upwelling of waters rich in biolimiting nutrients such as nitrogen, iron and phosphate (Wignall, 1994; Sinton and Duncan, 1997) and increased continental weathering leading to a discharge of nutrients into lakes and oceans (Jenkyns, 2010). As a result of this increase in organic productivity and subsequent anoxic conditions, there is as increase in total organic carbon (TOC) that is preserved in the sediment deposited during these events. OAEs are characterized by the sequestration of the lighter ^{12}C isotope present in organic matter, thus causing a reduction of ocean and atmospheric CO_2 (Arthur et al., 1988). The present study is focused around the OAE that occurred near the Cenomanian-Turonian (92-93 Ma)

boundary, known as OAE 2. This boundary is globally marked by a positive $\delta^{13}C$ excursion from 1.0‰-2.0‰ to 4.0‰-5.0‰ in carbonate due to the sequestration of the lighter ^{12}C in the burial and preservation of organic carbon and building of vast carbonate shelves (Schlanger et al., 1987).

1.2.3 Stratigraphy of the Eagle Ford Group

The mixed siliciclastic/carbonate Eagle Ford Group unconformably overlies the Buda Limestone and was deposited during a transgressive/regressive cycle on the oxygen-restricted Comanche Shelf (Haq et al., 1988) . The Austin Chalk unconformably overlies the Eagle Ford. The Buda Limestone and Austin Chalk are comprised of highly oxygenated carbonate sediments. The lower Eagle Ford is considered to represent the oxygen starved transgressive phase and is characterized by brittle, fissile black shales with a low number of species, a rarity of benthic organism and little bioturbation. The upper Eagle Ford is considered to be a regressive sequence and is characterized by interbedded shale, limestone and siltstone with a more diverse fossil assemblage (Dawson, 2000).

The earliest description of the Eagle Ford was made by Ferdinand Roemer in 1852, at which time he referred to it as “black shale with fish remains” (Harbor, 2011). R. T. Hill then established a type locality and named the formation after the town of Eagle Ford near Dallas, Texas and noted its occurrence within the Upper Cretaceous section of North Texas (Hill, 1901). The Eagle Ford Shale of northern East Texas was then subdivided, based on lithology, into the Tarrant, Britton and Arcadia Formations by W. L. Moreman (Sellards et al., 1932). Moreman also identified thickness trends within the upper Eagle Ford, in particular a thinning from about 100 feet near Dallas to 10 feet near

Austin. He also identified the contact with the overlying Austin Chalk to be an unconformity (Sellards et al., 1932).

In 1902 near Waco, Texas Prather named and established a type location for the South Bosque Formation and assigned it to the upper portion of the Eagle Ford in McLennan County, describing it as a marl below the Austin Chalk (Prather, 1902). The Lake Waco Formation was later described, underlying the South Bosque Formation as "brownish gray, flaggy limestone and dark to bluish gray, silty, calcareous shale with bentonite" (Adkins and Loza, 1951). Adkins (1924) included equivalent beds to the Pepper Shale as the base of the Eagle Ford, with the Buda Limestone lying unconformably underneath. In the Waco are, the Eagle Ford Group consists of the South Bosque representing the upper interval, while the Lake Waco and Pepper Shale constitute the lower interval.

Adkins and Lozo (1951) applied the term "Middle Flaggy Limestone" to the upper member of the Lake Waco Formation. This member was later identified as the Bouldin Member that had been described by Feray and Young (1949) in outcrop along West Bouldin Creek in Austin (Young, 1977). Young also described the Pepper Shale along a drainage ditch near the same creek (Fairbanks, 2012). Recent studies, namely Fairbanks (2012), has described the Waller Member as underlying the Bouldin Member within the Lake Waco Formation. The thickness of this member varies across the study area down to two feet thick and possibly even absent from some of the cores in the present study. Because the X-ray fluorescence scans for this study were performed at one foot intervals, the author does not feel the data would have sufficient resolution to accurately define the Waller Member.

In 1907, in West Texas, the sequence between the Buda Limestone and Austin Chalk was identified as the Boquillas Flags Formation (Udden, 1907). It was described

as “flaggy limestones with high organic and terrigenous content and low faunal diversity” (Udden, 1907; Donavan and Staerker, 2010). By the late 1950’s many geoscientists began to refer to the Boquillas as the Eagle Ford. In 1969 Pessagno divided the Boquillas Formation into an upper and lower middle, termed the Langtry and Rock Pens Members respectively. In recent studies (Lock and Peschier, 2006; Lock et al., 2007; Donavan and Staerker, 2010) the Langtry Member and Rock Pens Member terminology has been abandoned in favor of Langtry Formation and Eagle Ford Formation.

Biostratigraphic analyses of ammonites, foraminifera and nannofossils have positioned the Eagle Ford Group within the Cenomanian and Turonian stages (Scott, 1926; Pessagno, 1969; Jiang, 1989; Scott, 2010). The Cenomanian-Turonian boundary has been radiometrically dated to approximately 92 Mya and placed in the upper portion of the Eagle Ford Group (Dawson, 2000; Keller and Pardo, 2005)

This study will refer to the interval between the Austin Chalk and the Buda Limestone as the Eagle Ford Group (Figure 1.3). This group is subdivided, in descending order, into the South Bosque, Lake Waco and Pepper Shale Formations. The Pepper Shale and Lake Waco Formations represent the oxygen depleted, transgressive interval while the South Bosque Formation represents the high stand/regressive interval. The terms mudrock and shale are incorrectly used interchangeably in the literature (Kuypers, 2001; Kolonic et al., 2005; Hazel, 2008). Much of the Eagle Ford is enriched in calcium carbonate and does not possess the fissility associated with shale. Therefore the term mudrock will be utilized in this study.

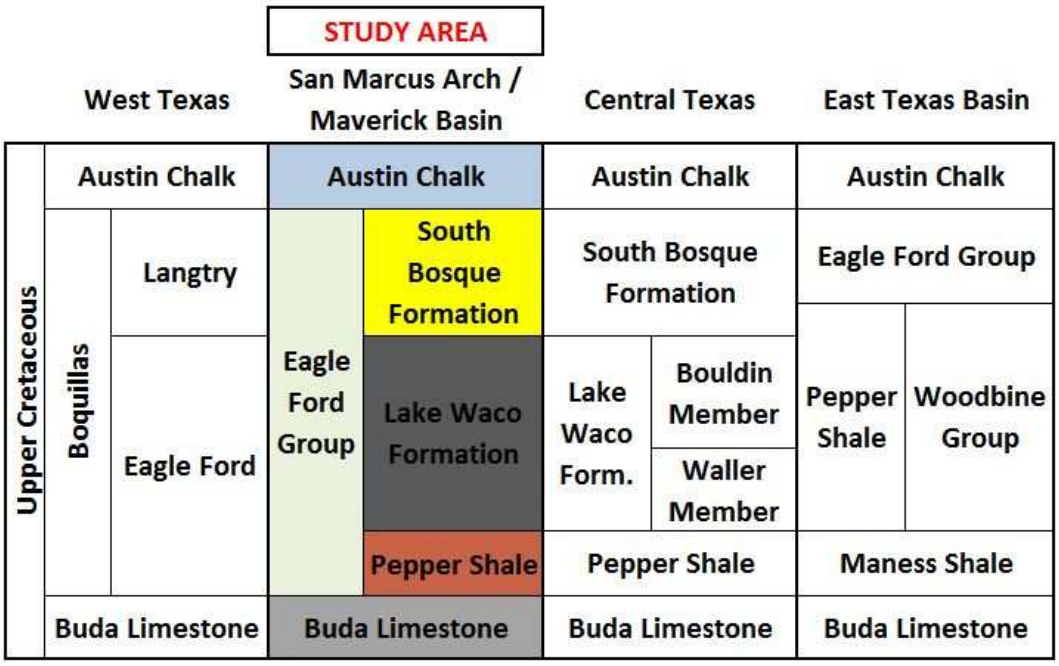

Figure 1.3 Stratigraphic column of the Eagle Ford Group. Modified from Harbor, 2011 and Fairbanks, 2012.

1.3 Economic Importance

Exploration of the Eagle Ford play began in La Salle County, Texas with a discovery well drilled by Petrohawk Energy in 2008 (Durham, 2010). This discovery became part of the Hawkeye Field, which now covers an area 15 miles north-south and 90 miles east-west. Early exploration focused on South Texas and extended from the Mexican border several counties into Texas (Durham, 2010). One property of the Eagle Ford that attracted exploration was the high calcite content that made the rock more brittle and susceptible to stimulated fracturing (Cherry, 2011). Early wells were predominately drilled in the down-dip, thermally very mature Eagle Ford and produced mainly dry gas and natural gas liquids. Exploration then spread northward, up-dip, into the less mature oil window. Activity then expanded into East Texas. It now covers an

area approximately 50 miles wide and 400 miles long from East Texas to the Mexican border, with an average thickness of 250 feet (Railroad Commission of Texas, 2014).

The Eagle Ford follows a northeast-southwest trend and is part of the Upper Cretaceous Gulfian Series. The oil and gas windows of this play suggest the hydrocarbons thermally mature in a southeastern direction. The Eagle Ford dips to the southeast from a depth of around 4000 feet at the northwestern extent to around 13,000 feet (Figure 1.4). There are currently 22 active fields covering 26 counties. Interest and production in the Eagle Ford has increased dramatically every year since its 2008 discovery (Figure 1.5 and Figure 1.6).

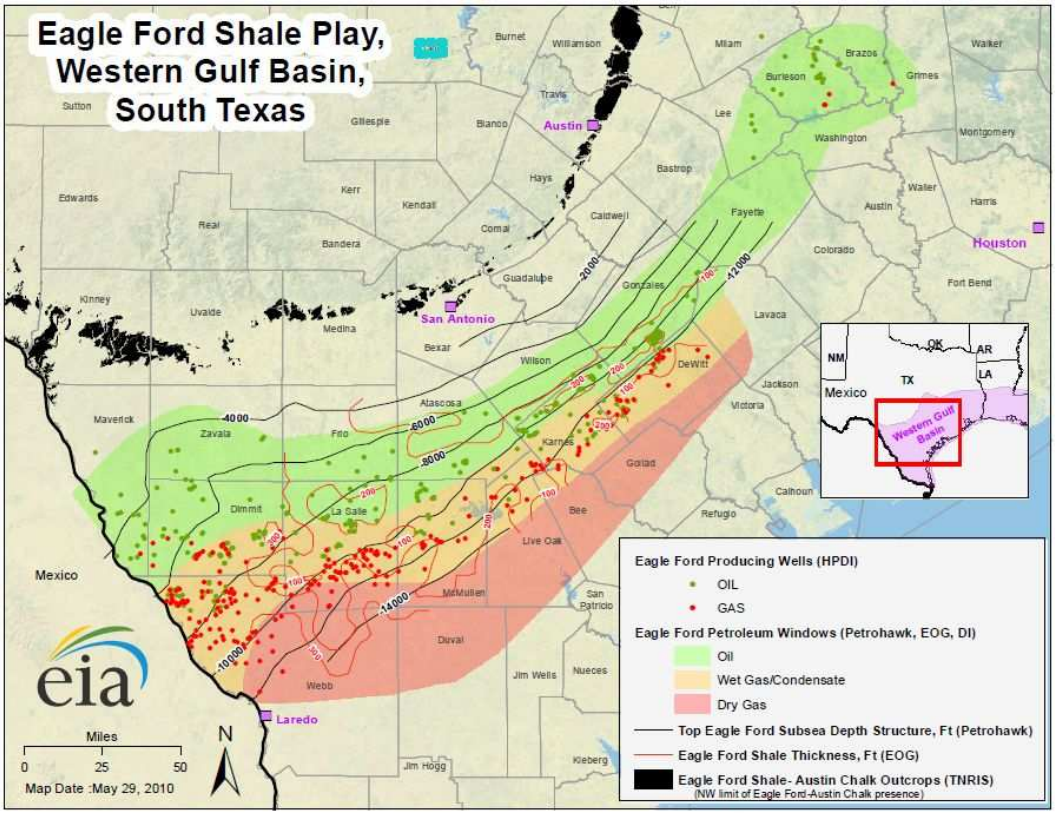

Figure 1.4 Map of Eagle Ford play, South Texas, with oil and gas window, and structural contours. Texas Railroad Commission (2014)

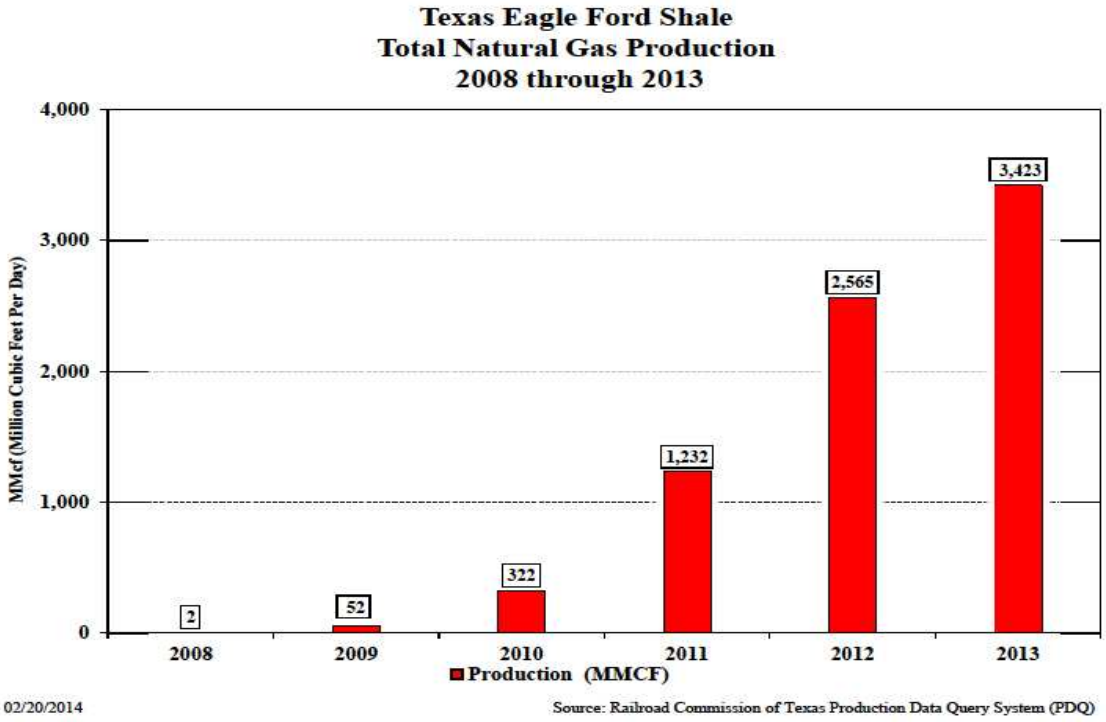

Figure 1.5 Total natural gas production in the Eagle Ford, 2008-2013. After Texas Railroad Commission (2014).

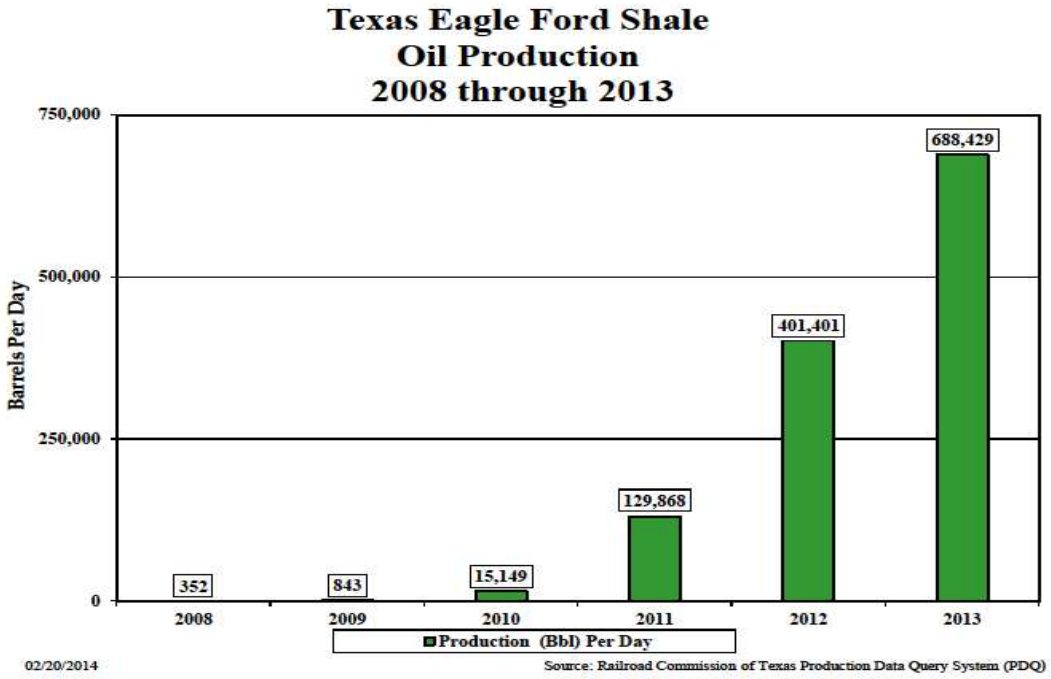

Figure 1.6 Total oil production in the Eagle Ford, 2008-2013. After Railroad Commission of Texas (2014).

1.4 Research Objectives

The objectives of the present study are to 1) develop chemostratigraphic records from multiple cores representative of the Eagle Ford Group of South Texas, 2) utilize the geochemical and chemostratigraphic results to develop a more comprehensive understanding of temporal and spatial variability in sub-environments and depositional conditions before, during and after the proposed OAE2 episode, and 3) generate a better perspective for how to utilize the results for oil and gas exploration and production.

Chapter 2

Methods

2.1 Core Information

A series of six drill cores from the Eagle Ford Formation in South Texas were analyzed. The cores were drilled in Gonzales, Guadalupe, La Salle and Wilson Counties in Texas. All of the drill cores are housed at the Core Research Center of the Texas Bureau of Economic Geology in Austin, Texas. Table 2.1 has general information for each of the cores analyzed. Figure 2.1 is a map of the distribution and major structural features of the Eagle Ford as well as core locations. Figure 2.2 is a map featuring a closer view of the core locations with the core names.

Table 2.1 General Core Information

Core Name	County (TX)	API #	Core Depth analyzed (ft.)	Core Lengths analyzed (ft.)
Blumberg, Jane W. #1-B	Guadalupe	42187305320000	4157-4228	71
Brechtel, Wayne #1	Wilson	42493302080000	3273-3316	43
Hendershot, Clare J. #1	Gonzales	42177302180000	4734-4777	43
Krause, A.L. estate #2	La Salle	42283302740000	9940-10001	61
Orts, H.P. #2	Gonzales	42177302030000	7680-7760	80
Shanklin, W.R. #1A	Guadalupe	42187015980000	2102-2147	45

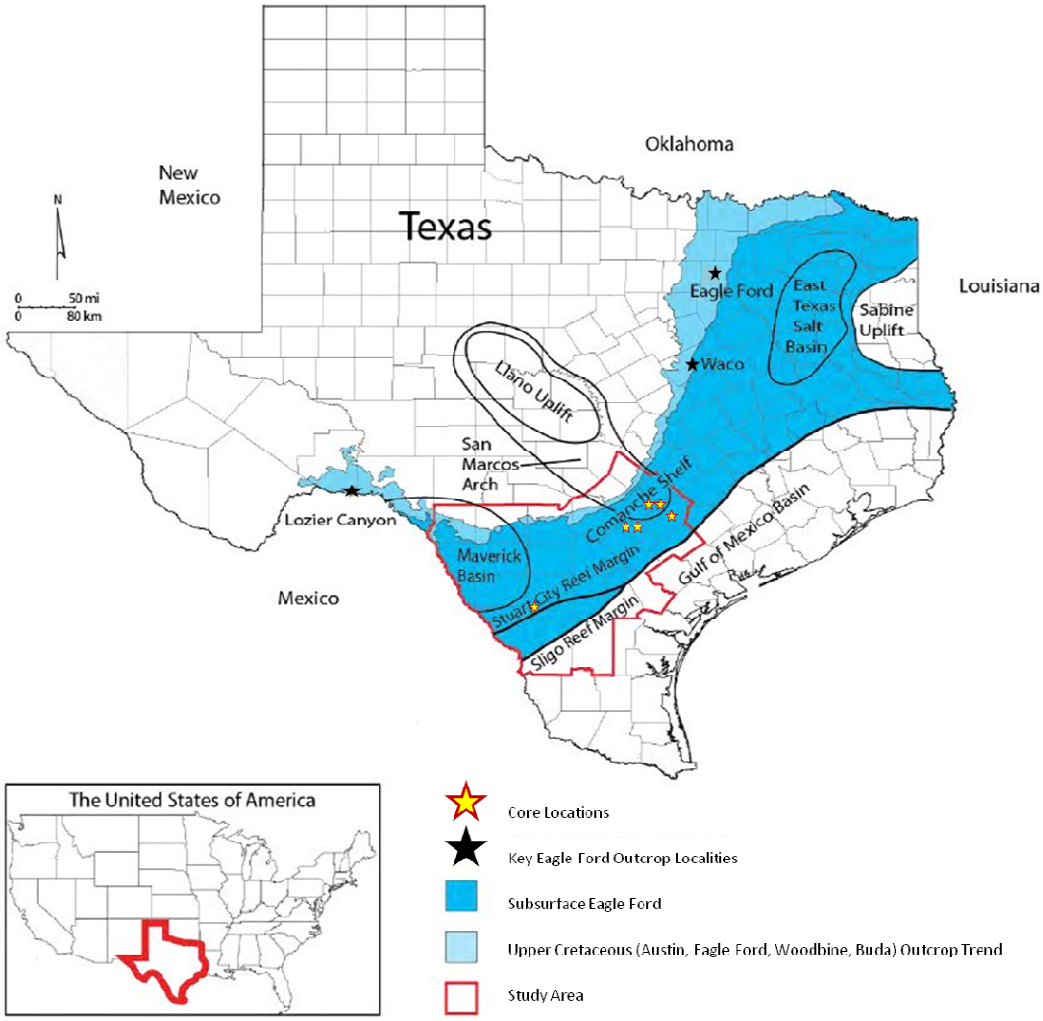

Figure 2.1 Map of study area showing distribution and major structural features of the Eagle Ford with core locations. Modified from Harbor (2011).

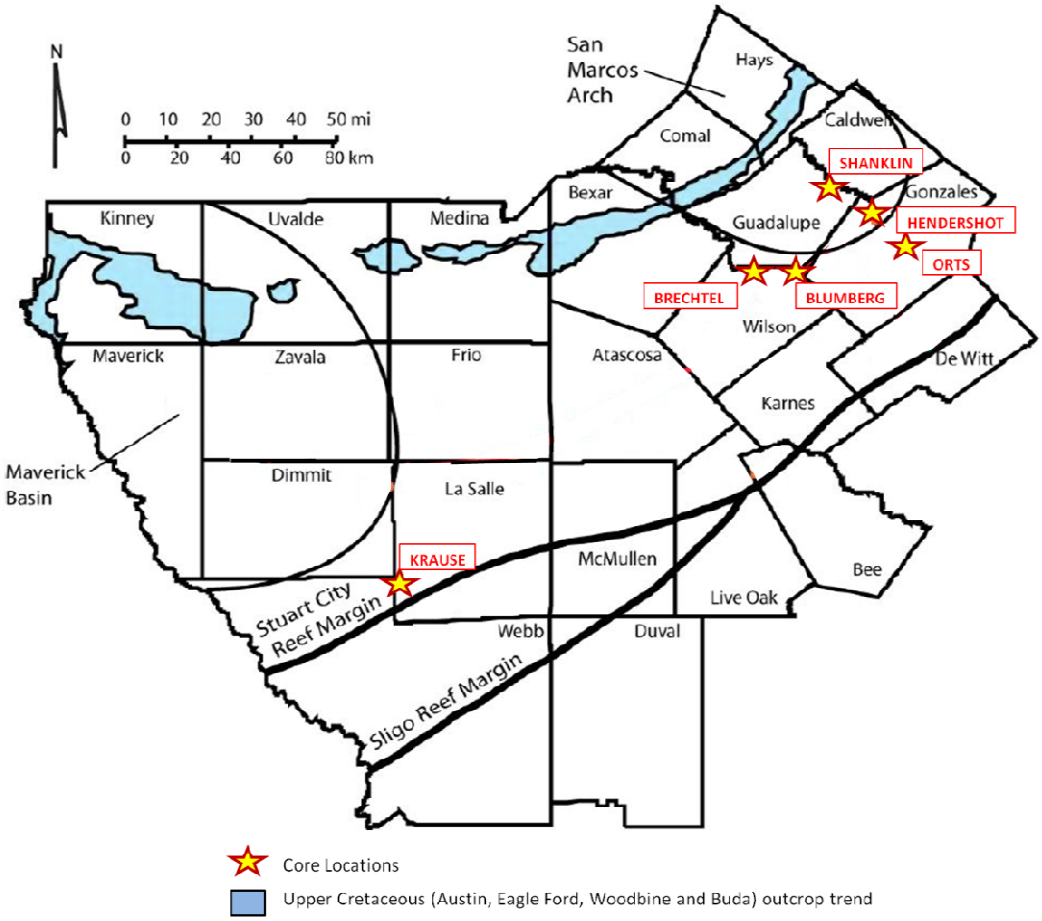

Figure 2.2 Map of study area with core names and locations. Modified from Harbor (2011).

2.2 Energy Dispersive X-Ray Fluorescence (ED-XRF)

2.2.1 ED-XRF Analysis

Core samples from six cores were marked at one-foot intervals prior to ED-XRF analysis. A Bruker Tracer III-V handheld ED-XRF spectrometer was used to measure elemental concentrations in each sample location. The instrument was stabilized using a plastic stand provided by Bruker. Samples were placed on the nose of the instrument immediately above the 3 by 4 mm elliptical beam window and stabilized using a platform that surrounded the nose of the instrument. The ED-XRF contains a silicon detector (SiPIN), located directly beneath the sampling window. The measurement sensitivity of the instrument decreases by the inverse square of the distance from this detector. In order to optimize the measurement consistency and accuracy, a flat sample surface is needed. Core samples were analyzed on the clean and dried, slabbed side whenever possible. Samples that were not suitably flat were given a flat surface area for analysis using a Dremel grinding hand tool.

Two phases of data acquisition were performed at each marked sampling location. Major element data acquisition, including V and Cr measurements, was undertaken using a low-energy, vacuum-pumped instrument setting. Trace element data acquisition was undertaken using a filtered, high-energy instrument setting. Each sample was analyzed for major and trace element concentrations for 180 seconds each. Major lithoclasts were avoided to minimize unrepresentative measurements.

Low-energy spectrum acquisition includes elements that emit characteristic x-rays between 1.25 and 7.06 kV. In order to obtain the elements in this range, and allow for backscatter that does not interfere with the peaks of interest, the voltage on the instrument was set to 15 kV. The instrument current was set to 42 μA. While the voltage settings remain constant for this elemental range, regardless of the Tracer III-V used, the

current settings vary between instruments because of inter-instrument variability associated with the manufacture of the x-ray tube and electronics. Instrument sensitivity to lighter elements (below and including Ca) was increased through the use of a vacuum pump attached directly to the Tracer III-V. This vacuum pump removes the air directly between the sampling window and the detector.

2.2.2 ED-XRF Mudrock Calibration

Calibration of the ED-XRF instrument for both major and trace elements was undertaken using a suite of ninety reference materials. These reference materials include: twenty from the Pennsylvanian Smithwick Formation of Central Texas, fifteen from the Late Cretaceous Eagle Ford Formation of South Texas, sixteen from the Mississippian Barnett Formation of North Central Texas, twenty-seven from the Devonian-Mississippian Woodford Formation of West Texas, seven from the Devonian-Mississippian Ohio Shale, and five international shale standards (Rowe et al., 2012).

Each reference material was pulverized to a 200 mesh powder using a TM Engineering pulverizer with trace metal grade stainless steel pulverizing cups and pucks. Approximately eight grams of each powdered reference material was pressed in a Carver press to forty tons with a forty millimeter die using a boric acid backing. The finished reference pellets were analyzed for major and trace elements using wavelength-dispersive X-ray fluorescence (WD-XRF) and inductively-coupled plasma mass spectrometry (ICP-MS), respectively.

The standard pellets were analyzed on the Bruker Tracer III-V for six minutes at three different locations on the pellet face under both low and high energy settings. All 270 raw x-ray spectra (90 references x 3 analyses) were loaded into Bruker's CalProcess software along with the accepted (WD-XRF & ICP-MS) elemental concentrations for all

standards. A low-energy and a high-energy calibration were developed by making inter-element corrections (slope and background) for each element in each calibration. Certain standards were omitted after the implementation of the inter-element corrections using statistical analysis for each element to determine the outliers with a standardized value greater than 3.0 standard deviations from the mean.

The completed calibration yields quantified values using the raw ED-XRF spectra from unknown samples. The low energy calibration quantifies the following elements: Mg, Al, Si, P, S, K, Ca, Ba, Ti, V, Cr, Mn, and Fe. The high energy calibration quantifies the following elements: Ni, Cu, Zn, Th, Rb, U, Sr, Y, Zr, Nb, and Mo. The limits of determination of a method (LDM) for each element are provided in Table 2.2 (Rousseau, 2001).

Table 2.2 Lowest Detectable Measurements (LDM) for Elements Analyzed.

Element	Accepted Value[a]	Instrument 1 (UTA-1)			Instrument 2 (1st UTA-2)		
		Measured Value[b]	σ (n=7)[b]	LDM[c]	Measured Value[b]	σ (n=7)[b]	LDM[c]
Mg (%)	0.67	0.80	0.09	0.17	0.85	0.14	0.28
Al (%)	4.96	5.39	0.14	0.28	5.32	0.11	0.22
Si (%)	32.6	33.7	0.2	0.5	33.1	0.4	0.8
P (%)	0.07	0.05	0.03	0.07	0.09	0.03	0.06
S (%)	3.34	2.18	0.10	0.20	2.27	0.09	0.18
K (%)	2.07	2.31	0.09	0.18	2.22	0.07	0.14
Ca (%)	0.13	0.23	0.03	0.06	0.24	0.02	0.04
Ti (%)	0.23	0.27	0.02	0.04	0.27	0.02	0.03
Mn (%)	0.015	0.012	0.001	0.002	0.013	0.001	0.003
Fe (%)	2.93	2.55	0.06	0.12	2.52	0.06	0.13
Ba (ppm)	2090	1884	376	753	1706	300	600
V (ppm)	928	1114	68	137	1110	80	159
Cr (ppm)	110	98	13	26	106	14	27
Ni (ppm)	130	153	26	52	150	20	40
Cu (ppm)	83	147	20	40	87	12	23
Zn (ppm)	823	844	96	191	880	74	147
Th (ppm)	8.4	9	1	2	9	1	2
Rb (ppm)	122	123	12	25	131	12	25
U (ppm)	18.1	17	6	11	22	4	8
Sr (ppm)	75.5	87	5	10	93	9	18
Y (ppm)	35.4	34	3	5	36	2	4
Zr (ppm)	80.3	95	7	13	96	6	13
Nb (ppm)	9	9	1	2	9	1	2
Mo (ppm)	79	83	4	9	82	3	6

a - Values for major elements from lithium borate-fused disc analysis by WD-XRF at SGS; values for trace elements (ppm) from sodium borate fusion dissolution and analysis by ICP-MS.

b - Average HH-ED-XRF measured values (n=7) and standard deviations for reference material RTC-W-260, a black shale from Devonian Woodford Formation of West Texas.

c - Limit of Determination of a Method (LDM) calculated according to Rousseau (2001).

2.3 Additional Geochemical Analysis

2.3.1 Sample Preparation

Samples for additional analyses were collected from each analysis location at approximately one foot intervals on the back side of the 2/3 side of the slabbed core. Powder samples were drilled with a Dewalt hand drill using a 3/8 inch drill bit. The samples were then stored in capped plastic vials and analyzed at the University of Texas at Arlington.

2.3.2 Total Inorganic Carbon (TIC)

Samples were analyzed for their total inorganic carbon (TIC) content utilizing a UIC, Inc. coulometer equipped with a CM5230 acidification module. This coulometer has an average unknown standard deviation of less than 0.5 percent (Engelman et al., 1985). Samples were weighed out between 2 to 10 mg and acidified at 70° C with ten percent phosphoric acid (H_3PO_4). Table 2.3 lists the subset of samples that were analyzed for TIC using this method.

2.3.3 Stable Isotopes ($\delta^{13}C_{carb}$ and $\delta^{18}O_{carb}$)

Depending upon the %TIC of the sample, determined by the above procedure, approximately 200-500 µg of powder sample were weighed into LABCO Exetainer vials and capped. These vials were then purged with ultra high purity helium gas for three minutes each. Samples were then acidified with three drops of 100% phosphoric acid (H_3PO_4) and equilibrated at 50℃ for 13.5 hours. Samples were subsequently analyzed using a Thermo Finnigan GasBench II peripheral connected to a Thermo Finnigan Delta-V isotope ratio mass spectrometer (IRMS). An in-house standard (UTAH) calibrated to

Vienna-PDB was used to standardize stable carbon ($\delta^{13}C$) and oxygen ($\delta^{18}O$) isotopic results. Table 2.3 lists the subset of samples that were analyzed using this method.

2.3.4 Total Organic Carbon (TOC)

Total organic carbon (TOC) analysis was performed on powdered samples that were weighed into silver capsules (Costech Analytical, Inc. #41067) and acidified repeatedly with six percent sulfurous acid (H_2SO_3) in order to remove carbonate phases (Verardo et al., 1990). These samples were analyzed using a Costech 4010 elemental analyzer interfaced with a Thermo Finnigan Conflo IV device to a Thermo Finnigan Delta-V isotopic ratio mass spectrometer (IRMS). The average standard deviation was 1.07% for the TOC of USGS-40. Table 2.3 lists the subset of samples that were analyzed for TOC using this method.

Table 2.3 Types and Number of Analyses Performed by Core.

Core Name	XRF	%TIC	%TOC	$\delta^{13}C/\delta^{18}O_{TIC}$	$\delta^{13}C_{TOC}$	%N	$\delta^{15}N_{TN}$
Blumberg, Jane W. #1B	69	69	0	69	0	0	0
Brechtel, Wayne #1	44	0	0	0	0	0	0
Hendershot, Clare J. #1	51	51	0	51	0	0	0
Krause, A.L. estate #2	61	0	61	0	61	61	61
Orts, H.P. #2	81	81	0	81	0	0	0
Shanklin, W.R. #1A	46	46	0	46	0	0	0

Chapter 3

Results

3.1 General X-Ray Fluorescence Data

3.1.1 Core Chemostratigraphy

All the graphs presented in this section represent results of X-ray fluorescence spectrometry as described in Chapter two. All plots relative to core depth have their units expressed as weight percent (e.g. %Al), ratio (e.g. %Si/%Al) or as an enrichment factor (EF). Enrichment factors are used to express elemental ratios that are enhanced within samples relative to their natural abundance in the average gray shale (Wedepohl 1971, 1991). Enrichment factors are expressed per the following equation:

$$EF=(\text{element in ppm/Al in ppm})_{sample} / (\text{element in ppm/Al in ppm})_{standard}$$

Where EF>1 = enrichment and EF<1 = depleted

Figures 3.1 through 3.6 represent X-ray fluorescence data relative to depth for each of the six cores analyzed for the present study. These figures illustrate the chemostratigraphic relationship of the major elements of calcium (Ca), aluminum (Al) and silicon (Si). Si is represented by the ratio of %Si/%Al to determine areas of Si enrichment above the amount contained within the clays. This excess Si could be from detrital or biogenic sources. These figures also contain the enrichment factors of the redox sensitive trace elements of vanadium (V), zinc (Zn), nickel (Ni) and molybdenum (Mo). These trace metals are often used as indicators of paleoenvironments (Brumsack, 1989; Dean and Arthur, 1989; Tribovillard et al., 2006; Algeo et al., 2007; Algeo and Maynard, 2008; Piper and Calvert, 2009).

The oldest stratigraphic unit present in all cores is the Buda Limestone Formation. This limestone is characterized by an enrichment of Ca (%Ca>35%) and a depletion of Al (%Al<1%). The Pepper Shale formation lies unconformably atop the Buda. The Pepper Shale displays highly variable and oscillatory values of %Ca (between 5% and 35%) and %Al (between 2% and 8%). Above this, the Lake Waco Formation also displays an oscillatory nature, but generally has values that are much more constrained. The %Ca values are consistently between 20% and 35% while the %Al values vary between 1% and 4%. There are also variations in the %Si/%Al ratio, especially in the Orts core (Figure 3.2). Both the Pepper Shale and Lake Waco represent the Lower Eagle Ford interval of these cores and they both display high variability in trace metal EF values, particularly with Mo values in the range of 100-200. Above this lies the South Bosque formation with %Ca and %Al values similar to that of the Lake Waco, as seen in the Orts core (Figure 3.2), but with less variation in the Si content. The South Bosque represents the Upper Eagle Ford interval of these cores, but is not present in the Brechtel (Figure 3.5) or the Krause (Figure 3.6). Within this interval there is little variation in the EF values, with Mo values at negligible levels. The Austin Chalk formation lies above the South Bosque, except in the Shanklin (Figure 3.4) and the Krause (Figure 3.6), where it is not represented. The Austin Chalk is characterized by higher Ca (%Ca>30) and lower Al (%Al<2%) values.

In some instances EF values may be calculated to be dramatically high or low and plot well off the scale provided in the graph. This is a factor of how the EF values are determined by the equation provided at the beginning of this section. Being that the Al value is in the numerator of the ratio, if the clay content of the sample is extremely low the EF value may vary widely.

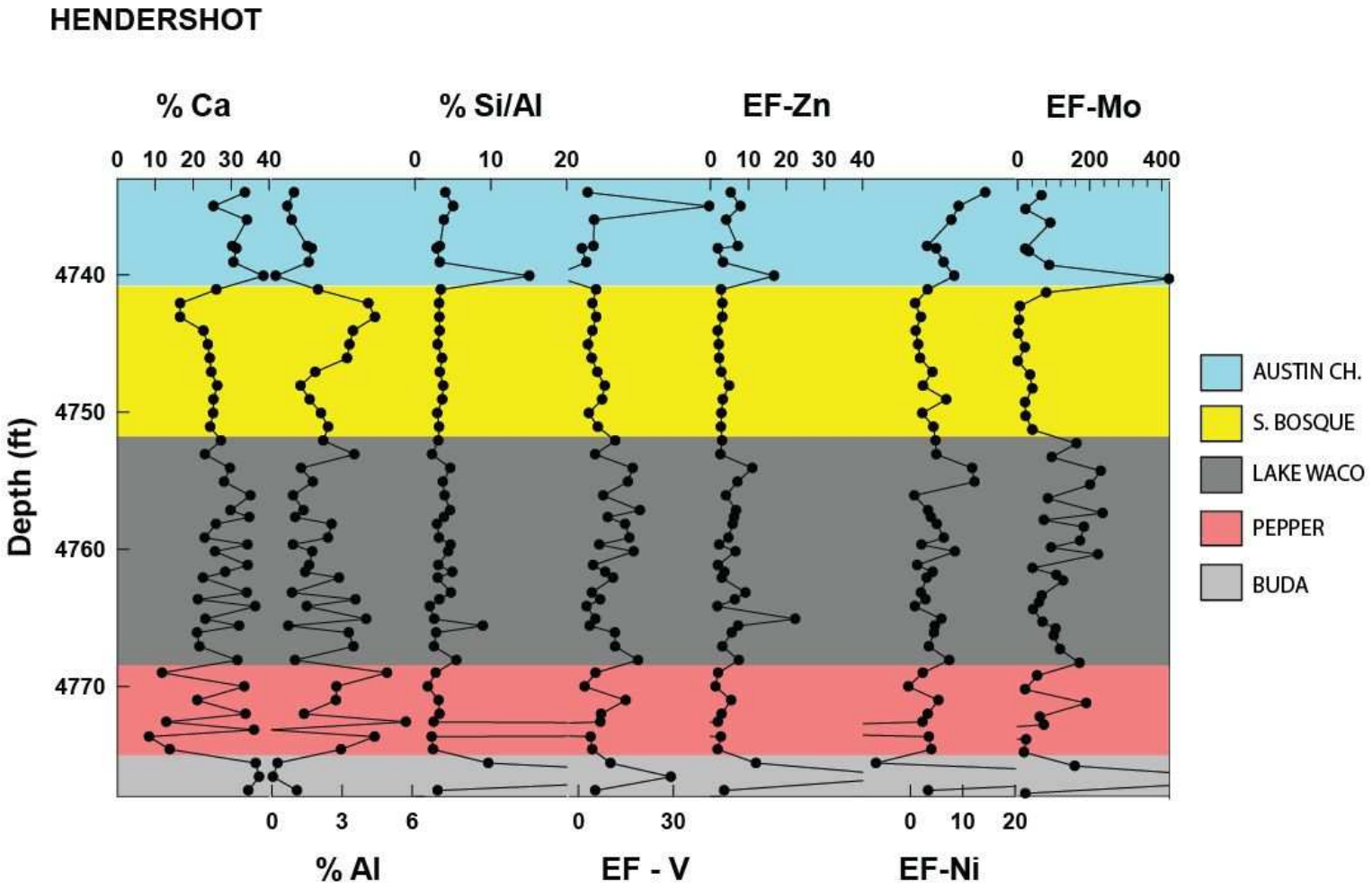

Figure 3.1 Major element and trace metal enrichment factor chemostratigraphy for Clare J. Hendershot #1 core.

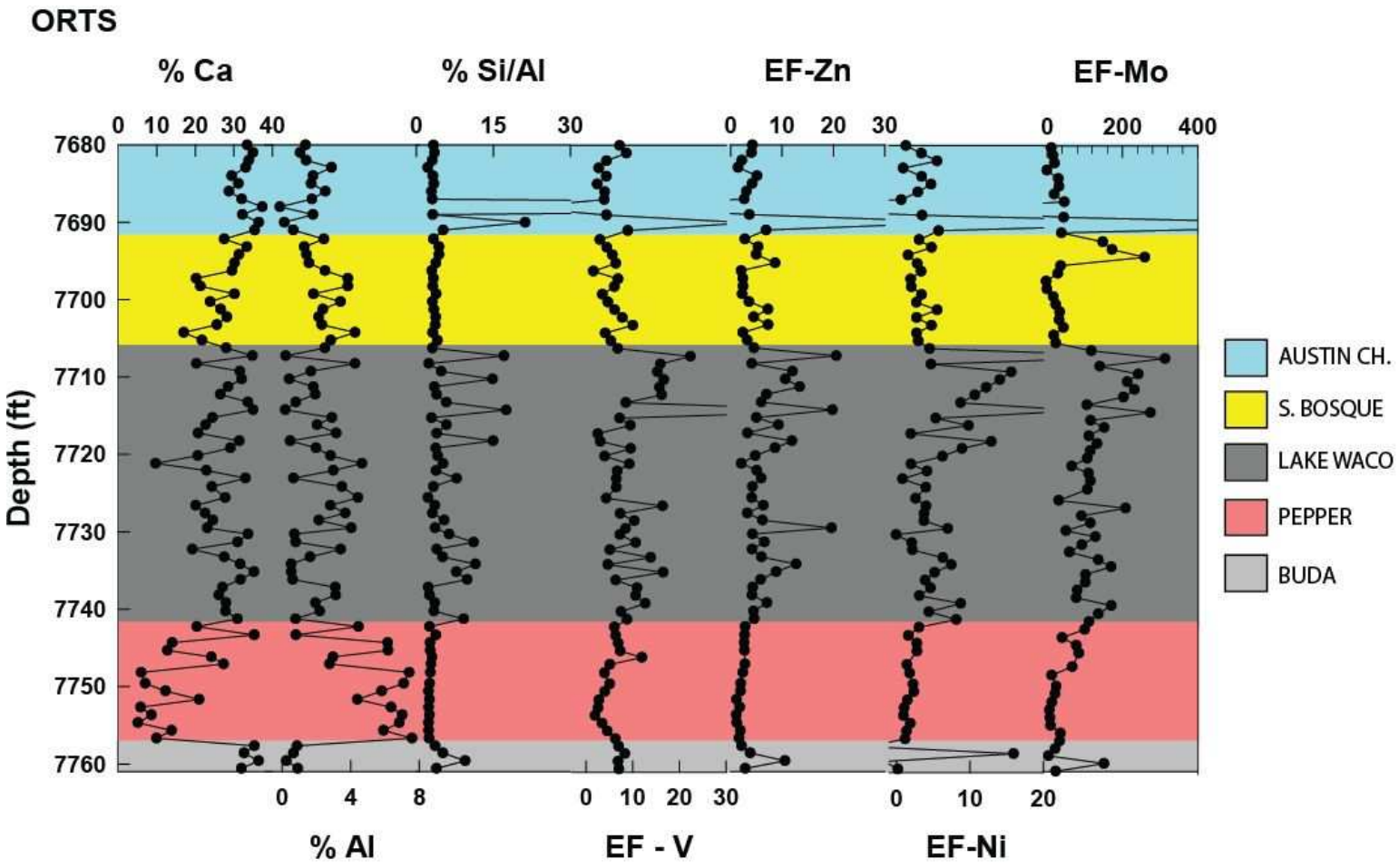

Figure 3.2 Major element and trace metal enrichment factor chemostratigraphy for H.P. Orts #2 core.

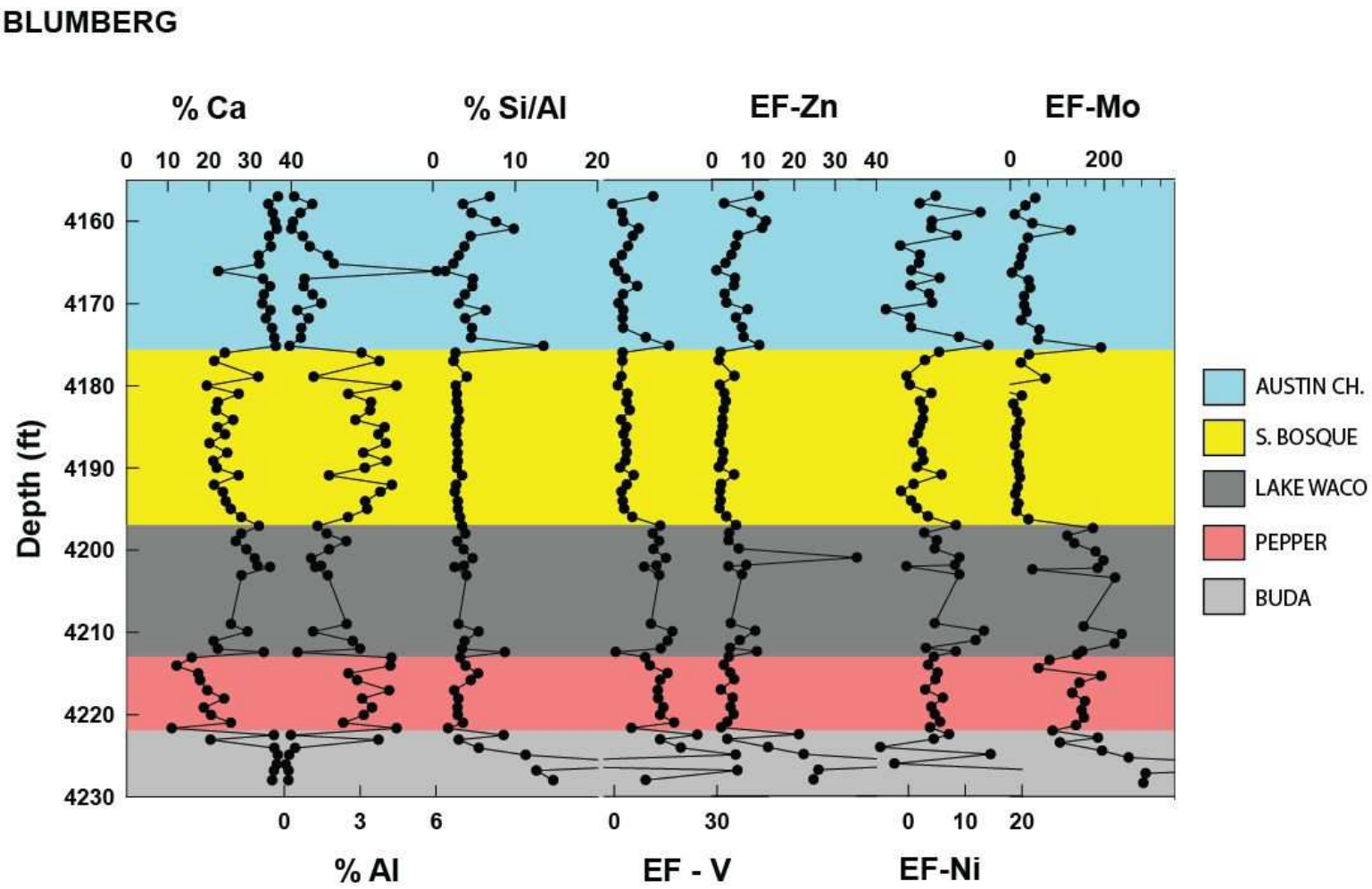

Figure 3.3 Major element and trace metal enrichment factor chemostratigraphy for Jane W. Blumberg #1-B core.

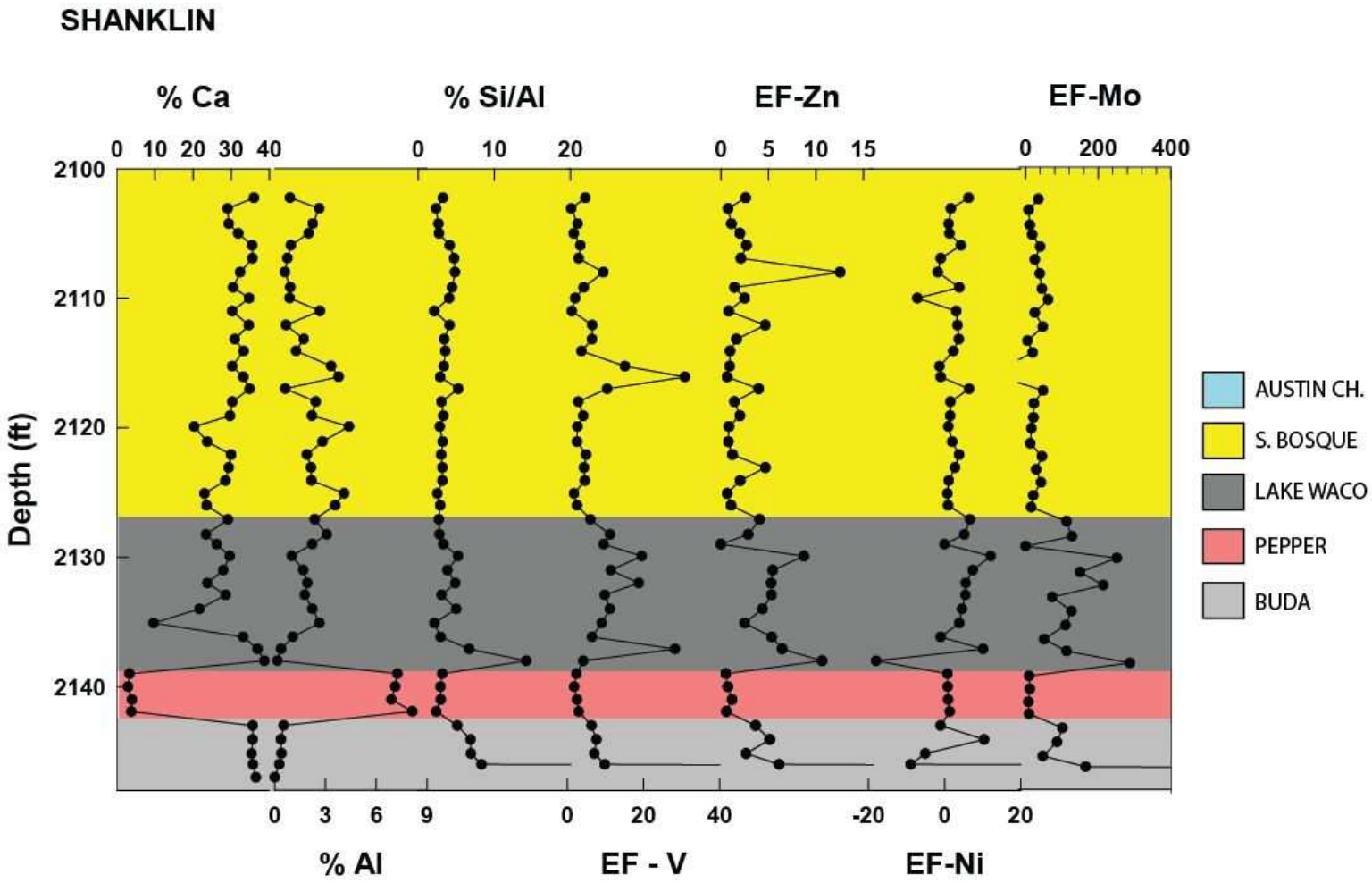

Figure 3.4 Major element and trace metal enrichment factor chemostratigraphy for W.R. Shanklin #1A core.

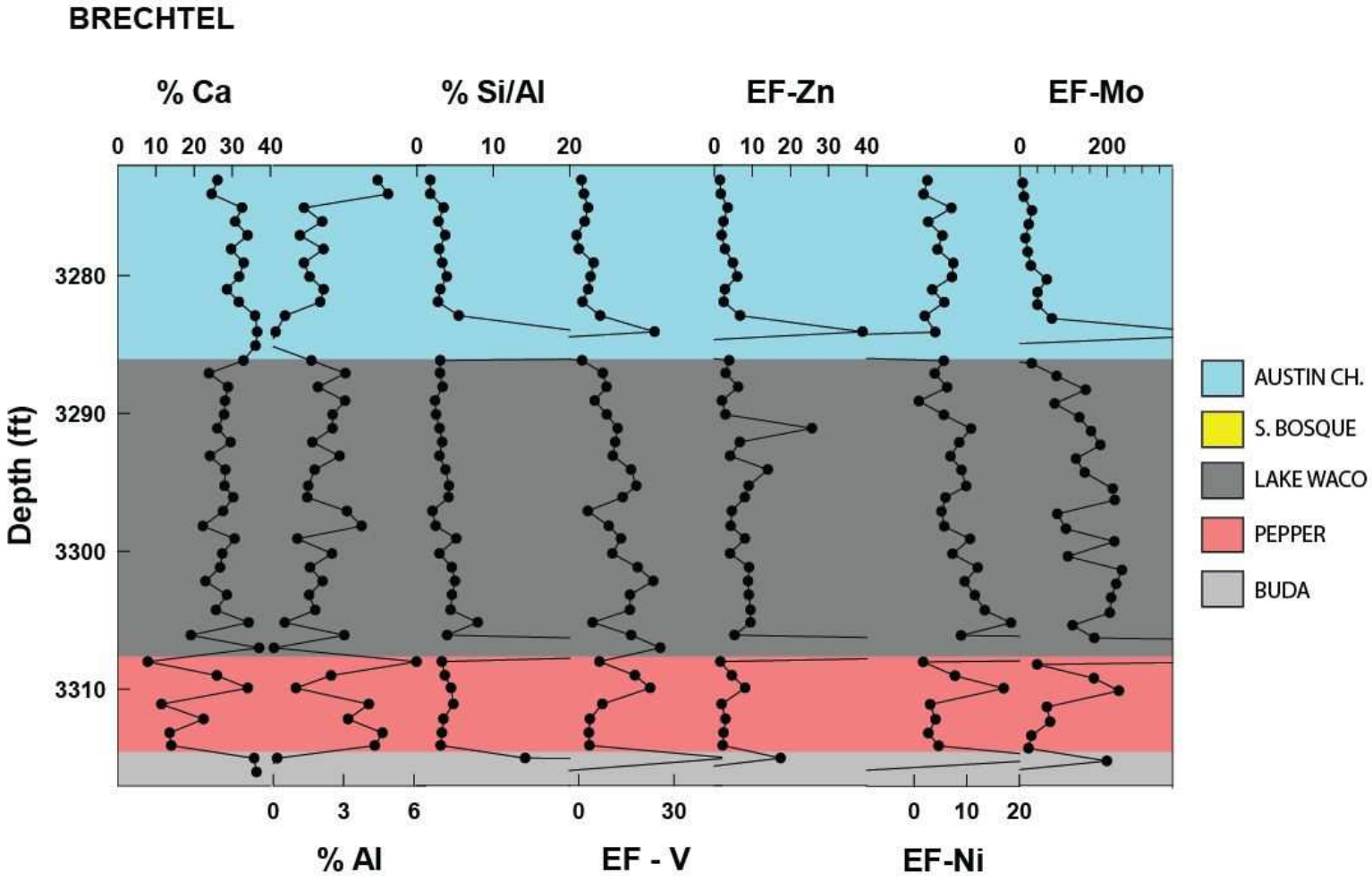

Figure 3.5 Major element and trace metal enrichment factor chemostratigraphy for Wayne Brechtel #1 core.

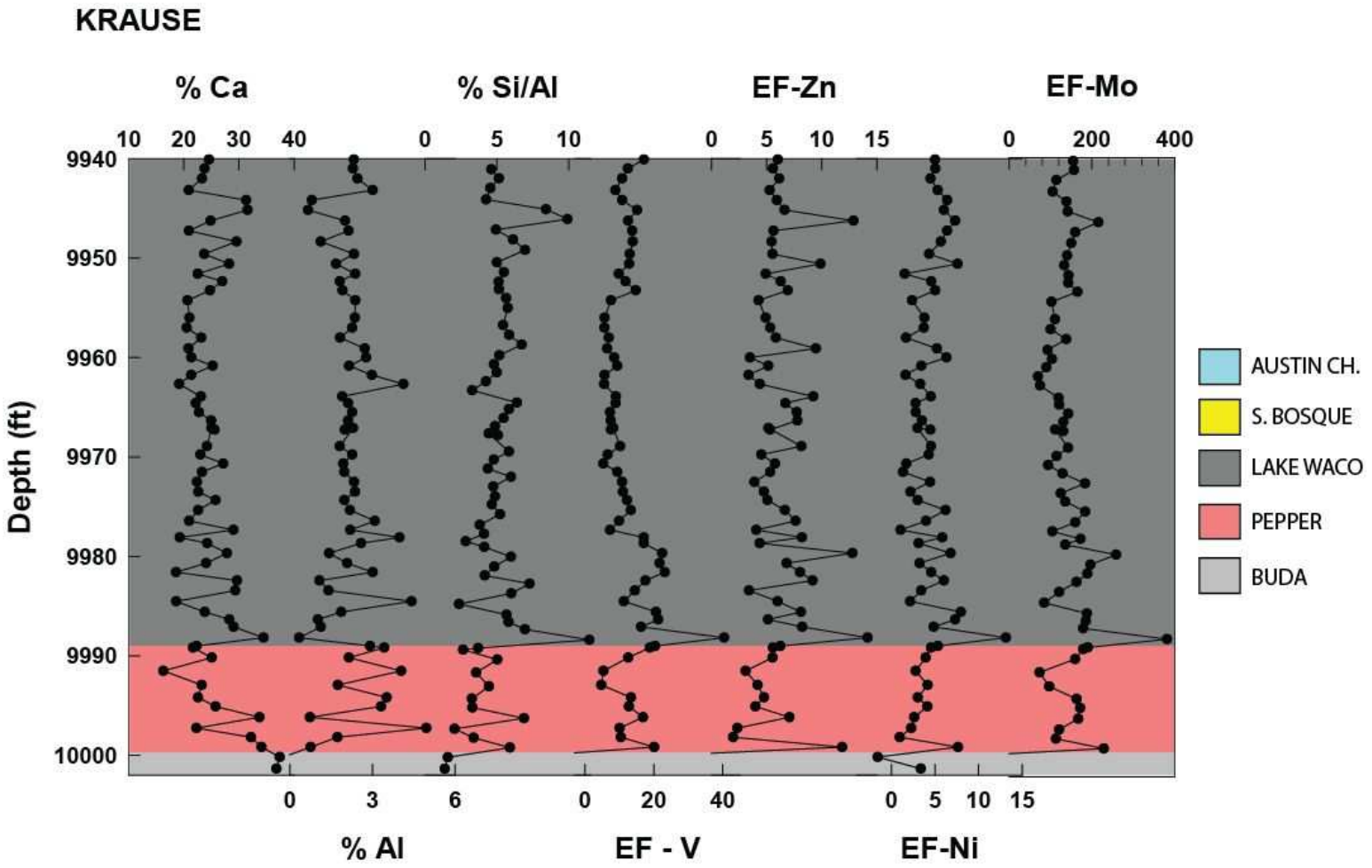

Figure 3.6 Major element and trace metal enrichment factor chemostratigraphy for A.L. Krause #2 core.

3.1.2 Calcite-Clay-Quartz Ternary Diagrams

Ternary diagrams utilizing calcium oxide (CaO), alumina (Al_2O_3), and silica (SiO_2) are used to compare the composition of the samples to that of the average marine gray shale, as defined by Wedepohl (1971, 1991). The solid red line on each plot represents a carbonate dilution line. All ternary diagrams were constructed with the use of normalized data. These normalized data represent the calcium, clay and quartz phases of the lithologic system.

Figures 3.7 through 3.12 are calcite-clay-quartz ternary diagrams for each of the six cores. All of the cores indicate varying degrees of carbonate dilution. Data from the Buda Limestone and Austin Chalk plot, as expected, more toward the calcite end member. The Pepper Shale samples display the least amount of carbonate dilution, such as can be seen in the Shanklin (Figure 3.7) and Orts (Figure 3.9). However, in the Krause core (Figure 3.12), the difference between the Pepper Shale and Lake Waco is not as obvious. In the four cores that possess data points within the South Bosque, Shanklin (Figure 3.7), Hendershot (Figure 3.8), Orts (Figure 3.9), and Blumberg (Figure 3.10), the Lake Waco displays more variability in the silica and clay components. Silica enrichment can be observed clearly in the Orts (Figure 3.9) and the Krause (Figure 3.12). It is not clear whether this excess silica is biogenic or detrital in origin.

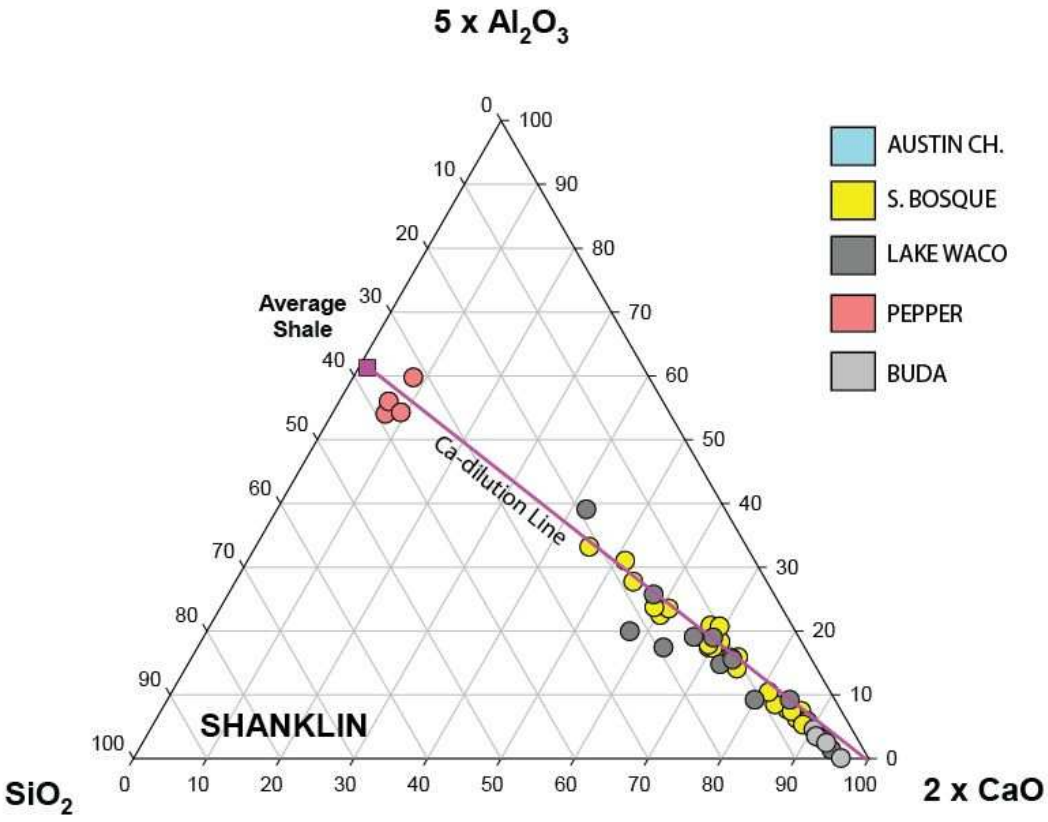

Figure 3.7 Calcite-Clay-Quartz ternary diagram for W.R. Shanklin #1A core

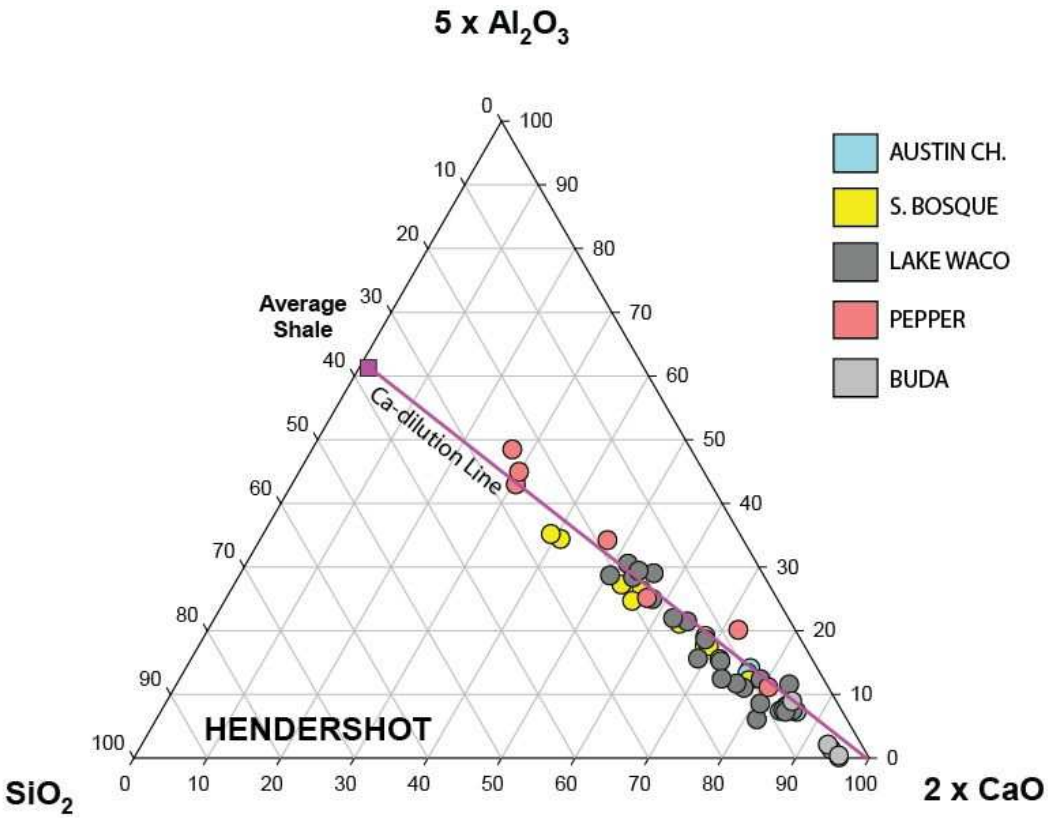

Figure 3.8 Calcite-Clay-Quartz ternary diagram for Clare J. Hendershot #1 core.

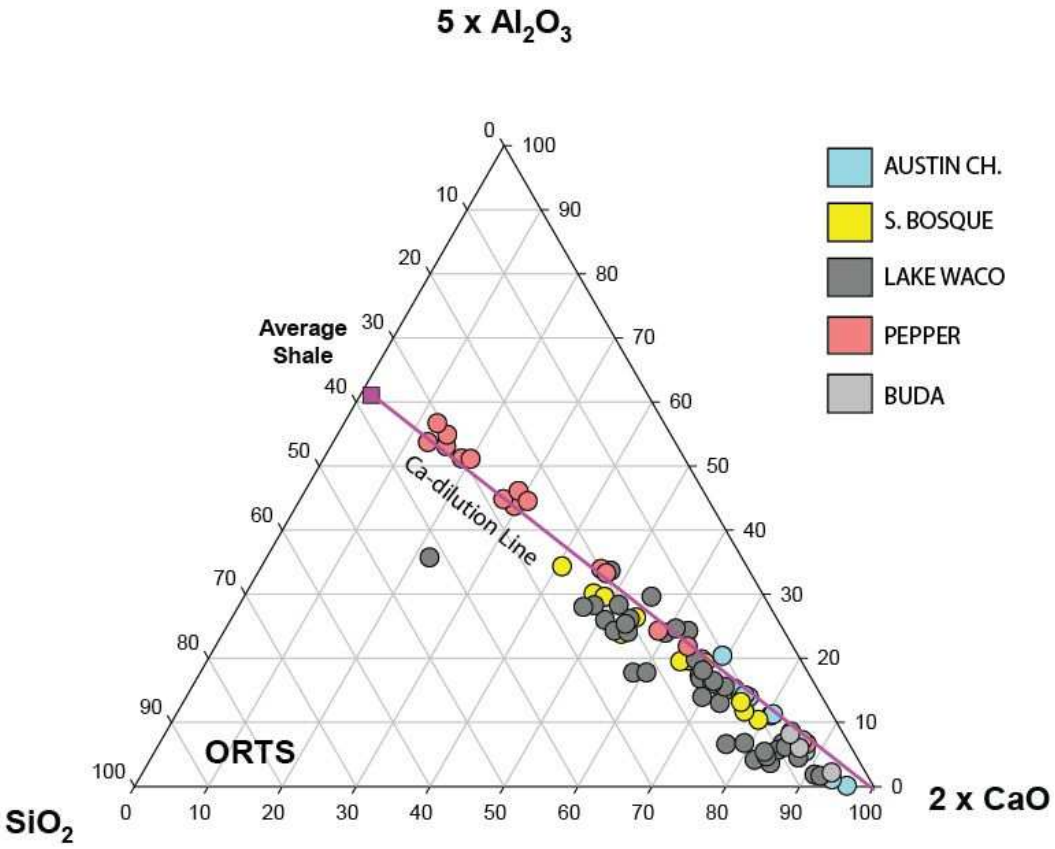

Figure 3.9 Calcite-Clay-Quartz ternary diagram for H.P. Orts #2 core.

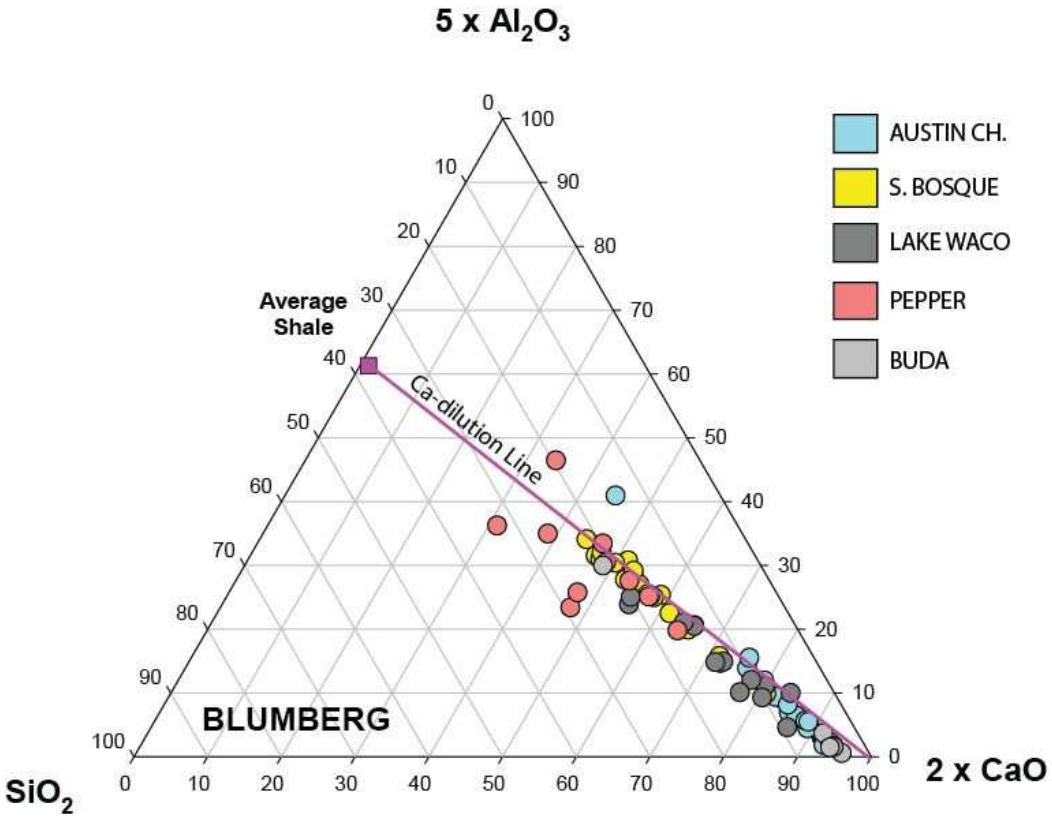

Figure 3.10 Calcite-Clay-Quartz ternary diagram for Jane W. Blumberg #1-B core.

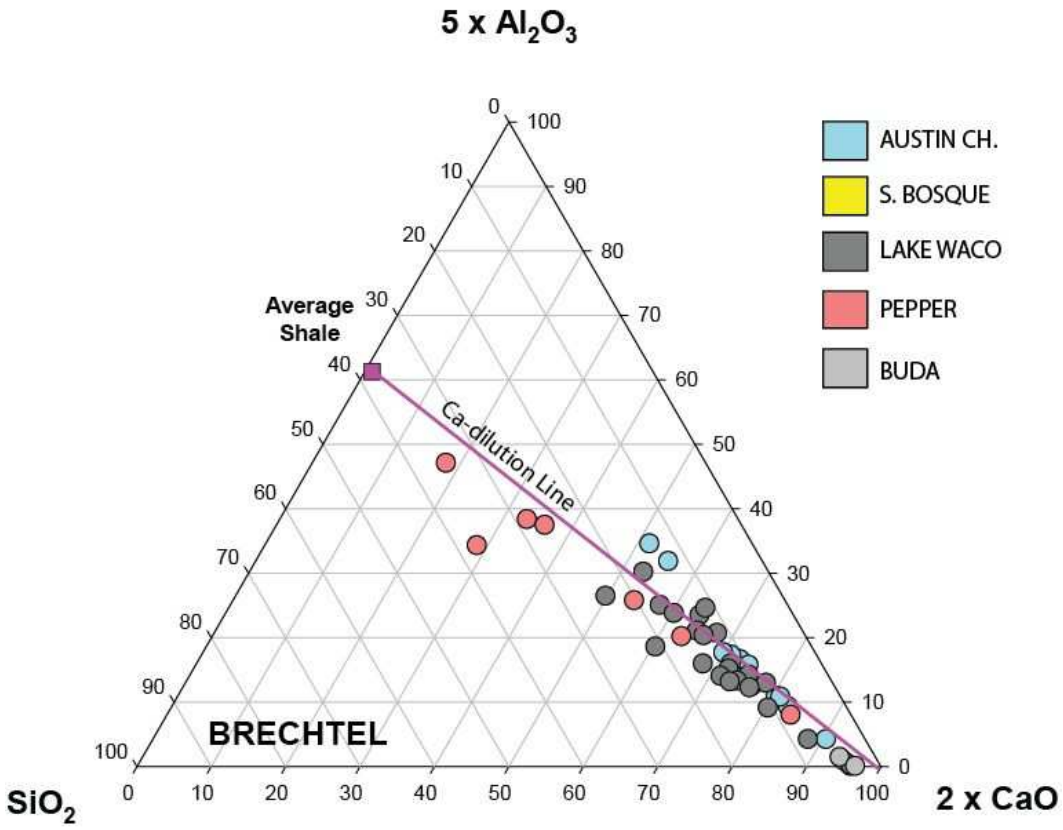

Figure 3.11 Calcite-Clay-Quartz ternary diagram for Wayne Brechtel #1 core.

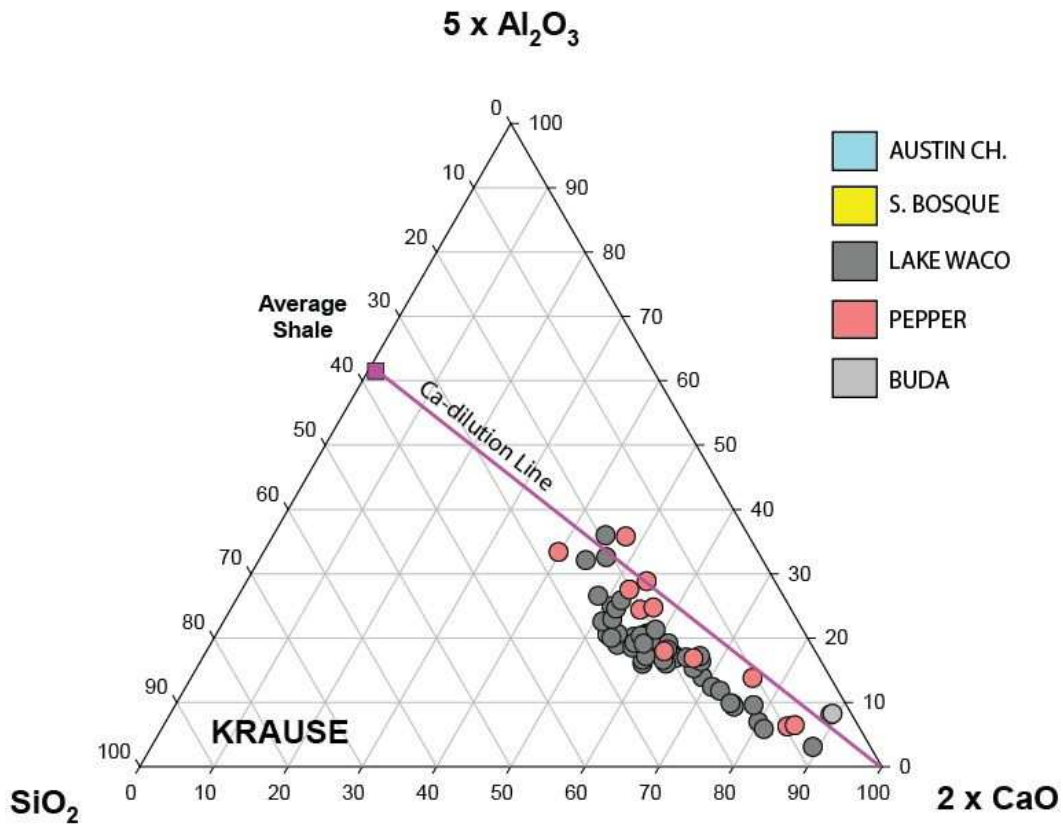

Figure 3.12 Calcite-Clay-Quartz ternary diagram for A.L. Krause #2 core

3.1.3 Elemental Cross-plots

The graphs presented in Figures 3.13 through 3.18 came from the X-ray fluorescence spectrometry described in Chapter two and are presented in weight percent (e.g. %Al).

Figure 3.13 contains the cross-plots of %Ca versus %Al for each of the six cores. Al is used as a proxy for the clay content while Ca is used to represent the carbonate component. The negative slope of the Ca relative to the Al suggests the clay content

was diluted by the carbonate deposition. The Buda Limestone and Austin Chalk tend to show higher Ca and lower Al. Conversely, the Pepper Shale displays higher Al and lower Ca, with the exception of the Krause core.

Figure 3.14 contains the cross-plots of %Si versus %Al for each of the six cores. A positive linear trend between these two elements indicates that the Si is contained within the clay (e.g. illite) component. A deviation above this trend suggests an enrichment of silica by either detrital (quartz) or biogenic (radiolarian) origin. Si enrichment can be seen in the Blumberg and Brechtel cores primarily in the Pepper Shale. This excess Si can also be observed the Lake Waco and South Bosque intervals of the Hendershot and Orts cores. The Krause core displays a general Si enrichment over most of the studied interval.

Figure 3.15 contains the cross-plots of %Ti versus %Al for each of the six cores. Ti is reflective of detrital inputs due to its ultra-low seawater abundance and lack of participation in biologic cycling. It is because of this that Ti is sometimes used, instead of Al, as a proxy for clay content. Deviations above the positive trend line suggest the presence of other Ti bearing, such as rutile or anatase (TiO_2).

Figure 3.16 contains the cross-plots of %K versus %Al for each of the six cores. A positive trend would indicate that K is associated with the main clay phase, illite in this case. Deviations above this trend could indicate the presence of another mineral phase, possibly K-feldspar ($KAlSi_3O_8$). Plots below this trend could indicate a change in clay chemistry from illite dominated to more rich in clays that do not contain K, such as smectite or kaolinite.

Figure 3.17 contains the cross-plots of %S versus %Fe for each of the six cores. A positive trend in this relationship would indicate the presence of pyrite, which can be used as an indicator of euxinic/sulfidic conditions at the basin floor and lower water

column. Pyrite can be seen with a physical inspection of these cores. However, the %S data obtained through the use of handheld XRF instruments can be unreliable. These plots are included below to illustrate the point that even though S is a very important redox indicator and is normally used in geochemical studies, these data will not be used to reach any conclusions in this study.

Figure 3.18 contains the cross-plots of %Ca versus %Mg for each of the six cores. This comparison is used to illustrate the relationship of Mg with carbonate phase. A higher percentage of Mg could indicate the possibility of another carbonate mineral such as ankerite ($Ca(Mg,Fe,Mn)(CO_3)_2$) or dolomite ($CaMg(CO_3)_2$).

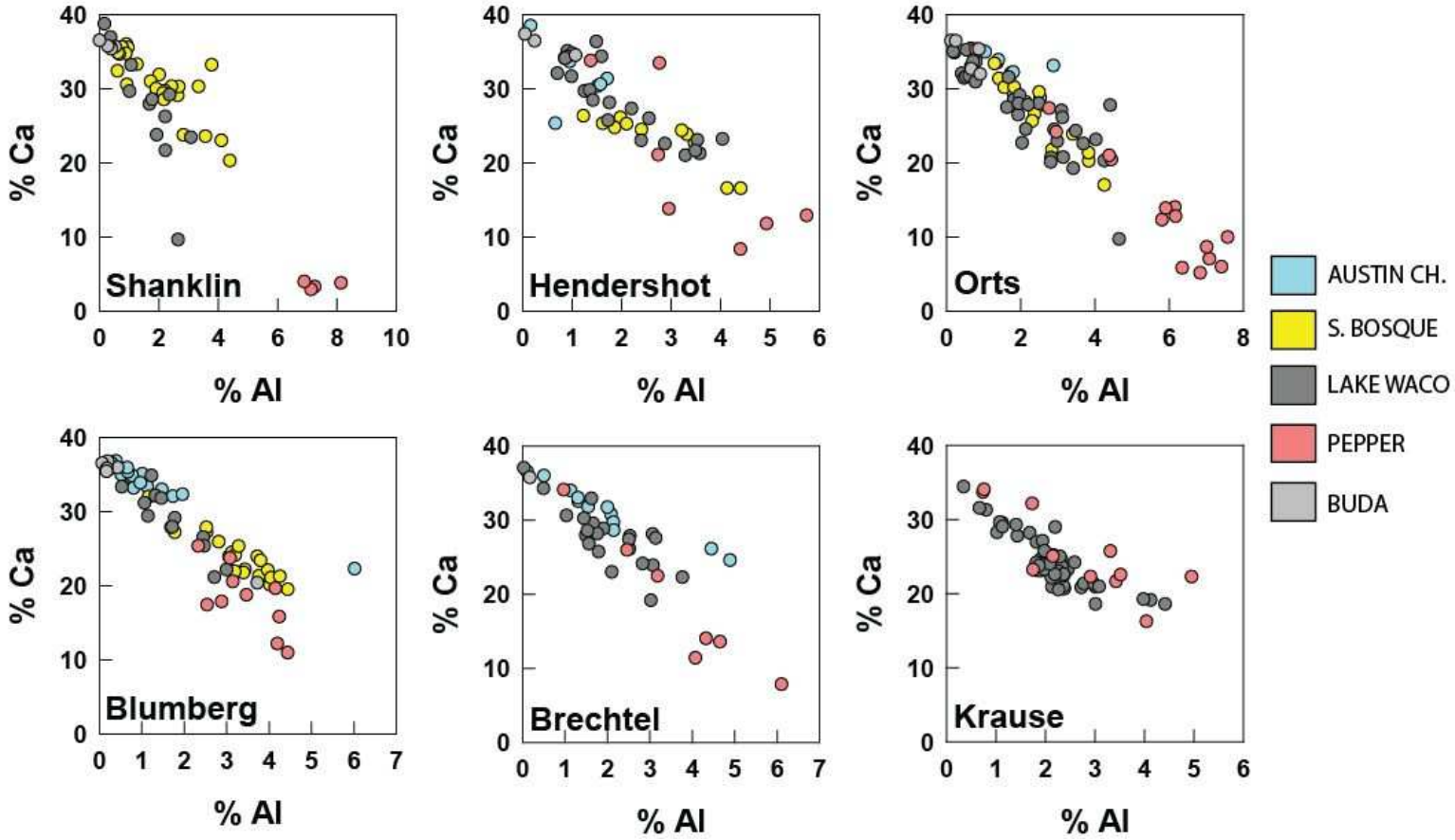

Figure 3.13 Calcium (%Ca) versus aluminum (%Al) cross-plots for all six cores.

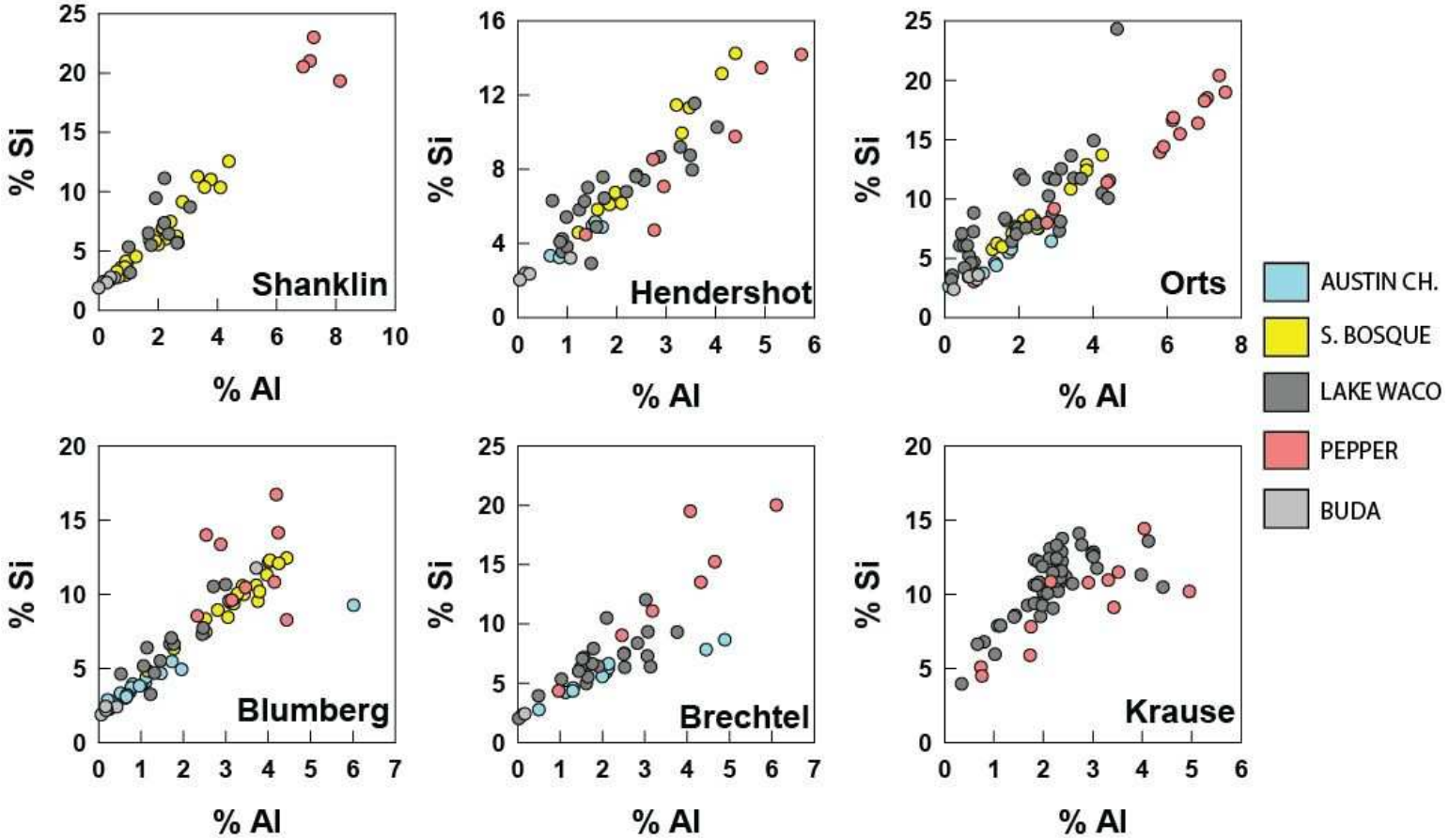

Figure 3.14 Silicon (%Si) versus aluminum (%Al) cross-plots for all six cores.

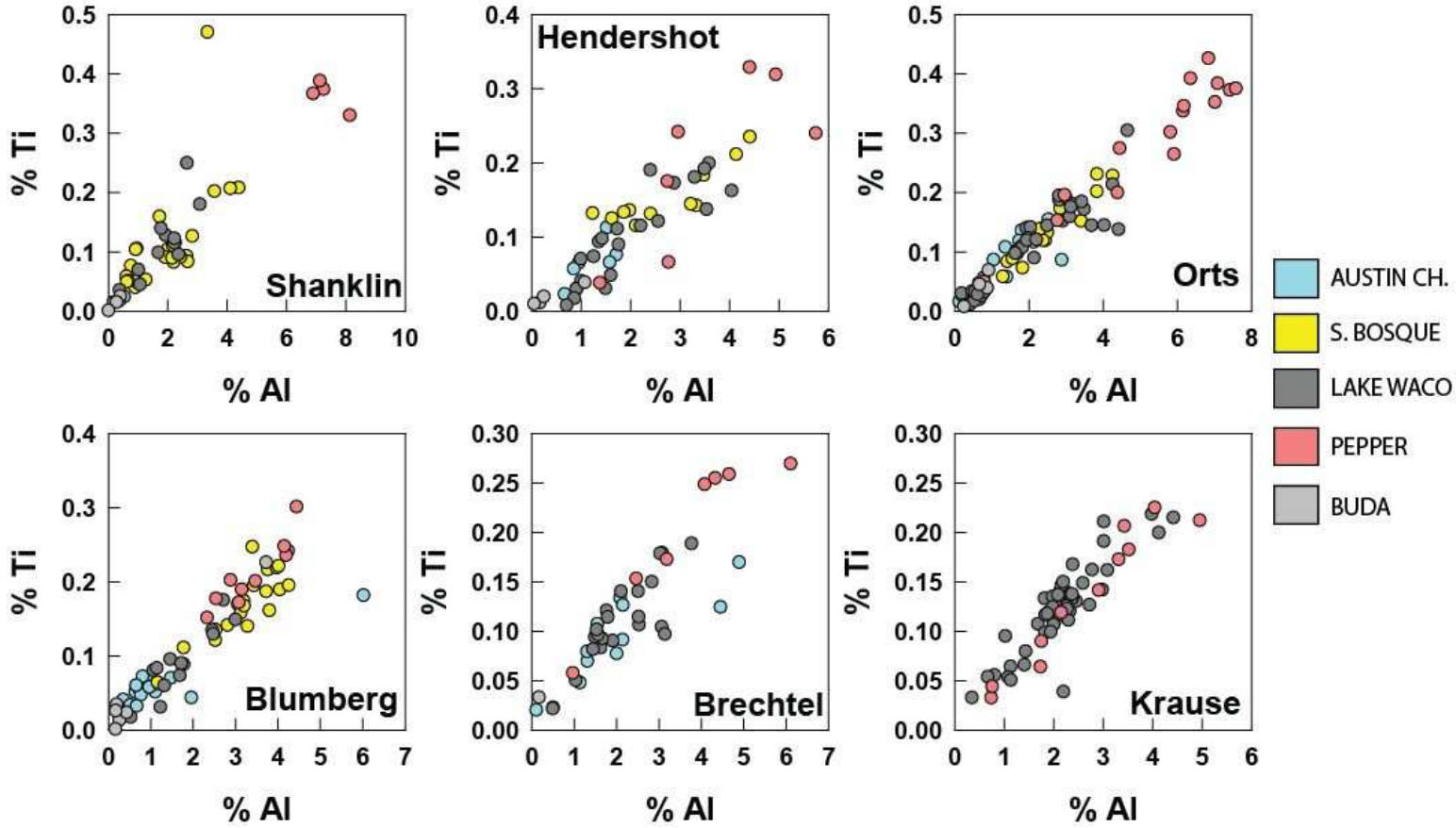

Figure 3.15 Titanium (%Ti) versus aluminum (%Al) cross-plots for all six cores.

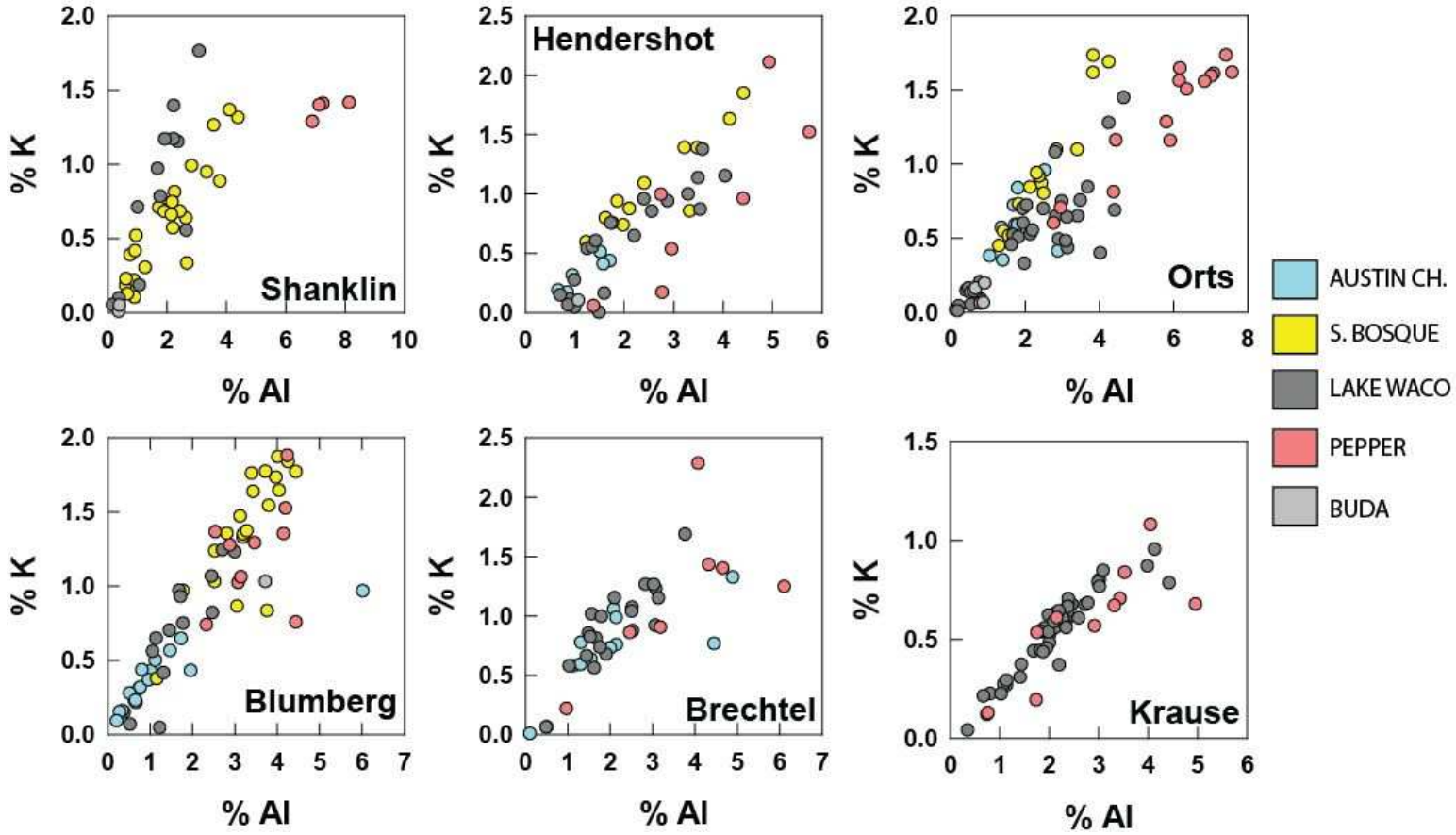

Figure 3.16 Potassium (%K) versus aluminum (%Al) cross-plots for all six cores.

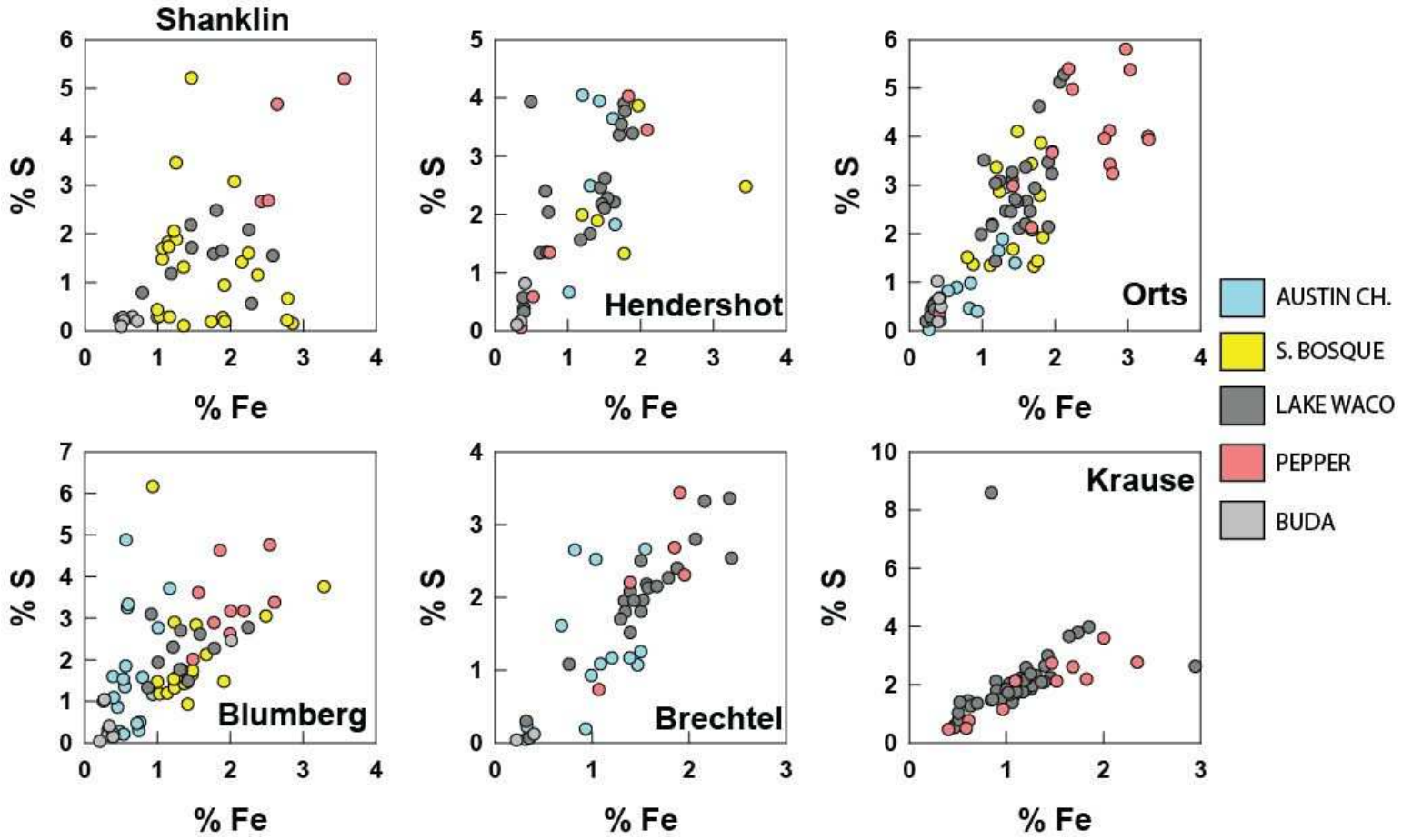

Figure 3.17 Sulfur (%S) versus iron (%Fe) cross-plots for all six cores.

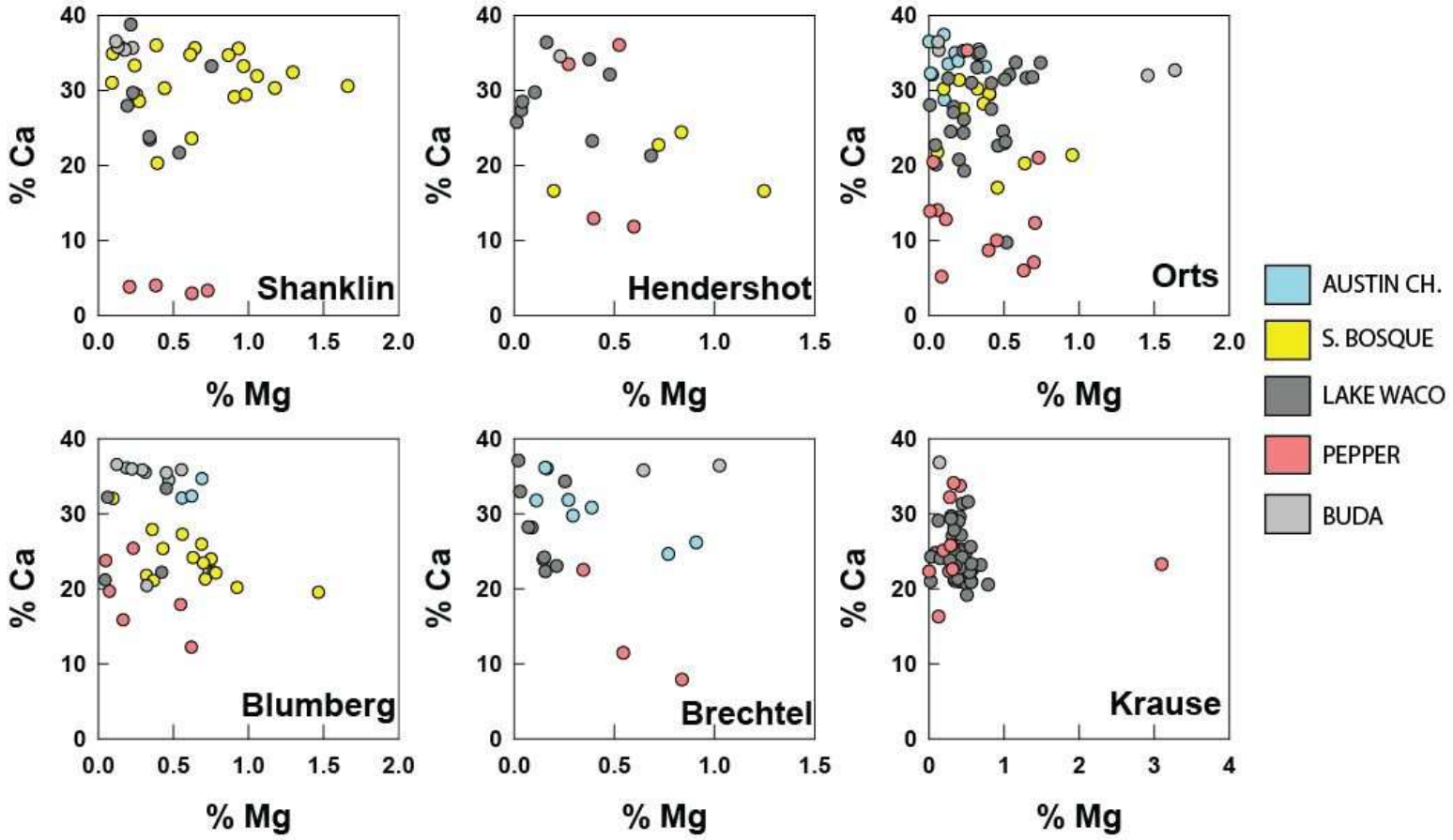

Figure 3.18 Calcium (%Ca) versus magnesium (%Mg) cross-plots for all six cores.

3.2 Non XRF Data

3.2.1 Total Organic Carbon (TOC)

Total organic carbon (TOC) measurements are presented in total weight percent (%TOC). Figure 3.19 displays %TOC levels Krause core. The portion of the Krause core analyzed in this study only contains the Lake Waco and Pepper Shale formations that constitute what is considered to be the Lower Eagle Ford. Values are predominately around 5% with an abrupt decrease at the lowest portion of the Lake Waco Formation.

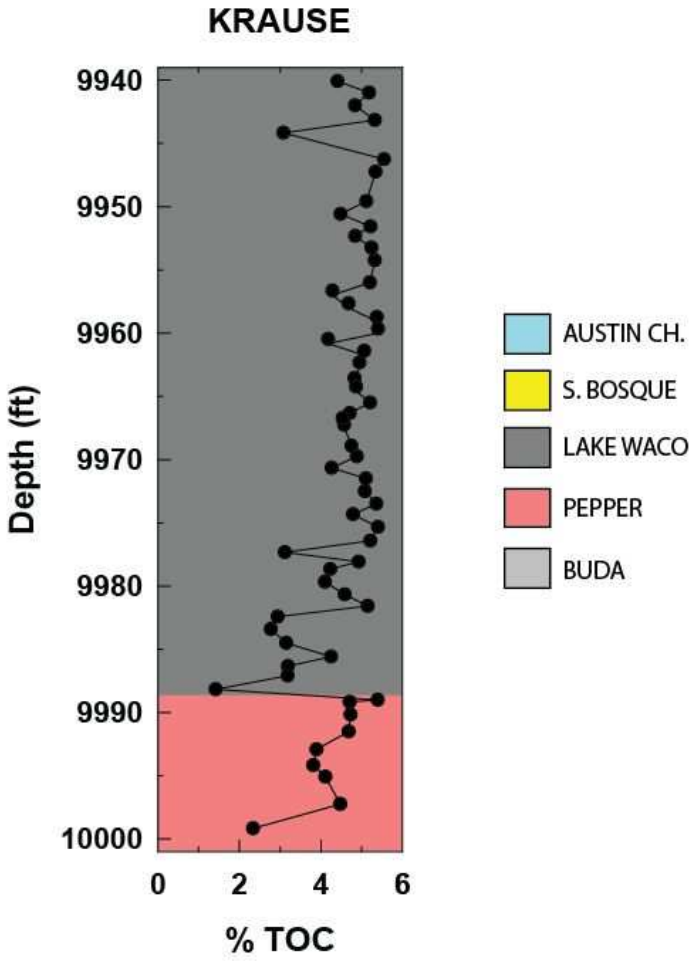

Figure 3.19 %Total organic carbon versus depth for the A. L. Krause #2 core.

3.2.2 Stable Carbonate Isotopes

Stable isotope measurements of $\delta^{13}C$ and $\delta^{18}O$ for carbonate are presented as per mil (‰). Figure 3.20 contains the carbonate isotope values for the Blumberg, Orts, Hendershot and Shanklin cores. Changes in $\delta^{18}O$ values have mainly been interpreted as changes in temperature, with positive excursions representative of cooling periods. Such a positive excursion could be interpreted as an increase in snowfall or development of polar ice creating a draw down in availability of the lighter ^{16}O isotope. Positive and negative excursions of the $\delta^{13}C$ curve can be used to identify such things as periods of increased organic carbon preservation. A positive excursion in the $\delta^{13}C$ signal can usually be observed during periods of oxygen depletion or anoxia, due to the sequestering of the lighter ^{12}C isotope within preserved organic matter.

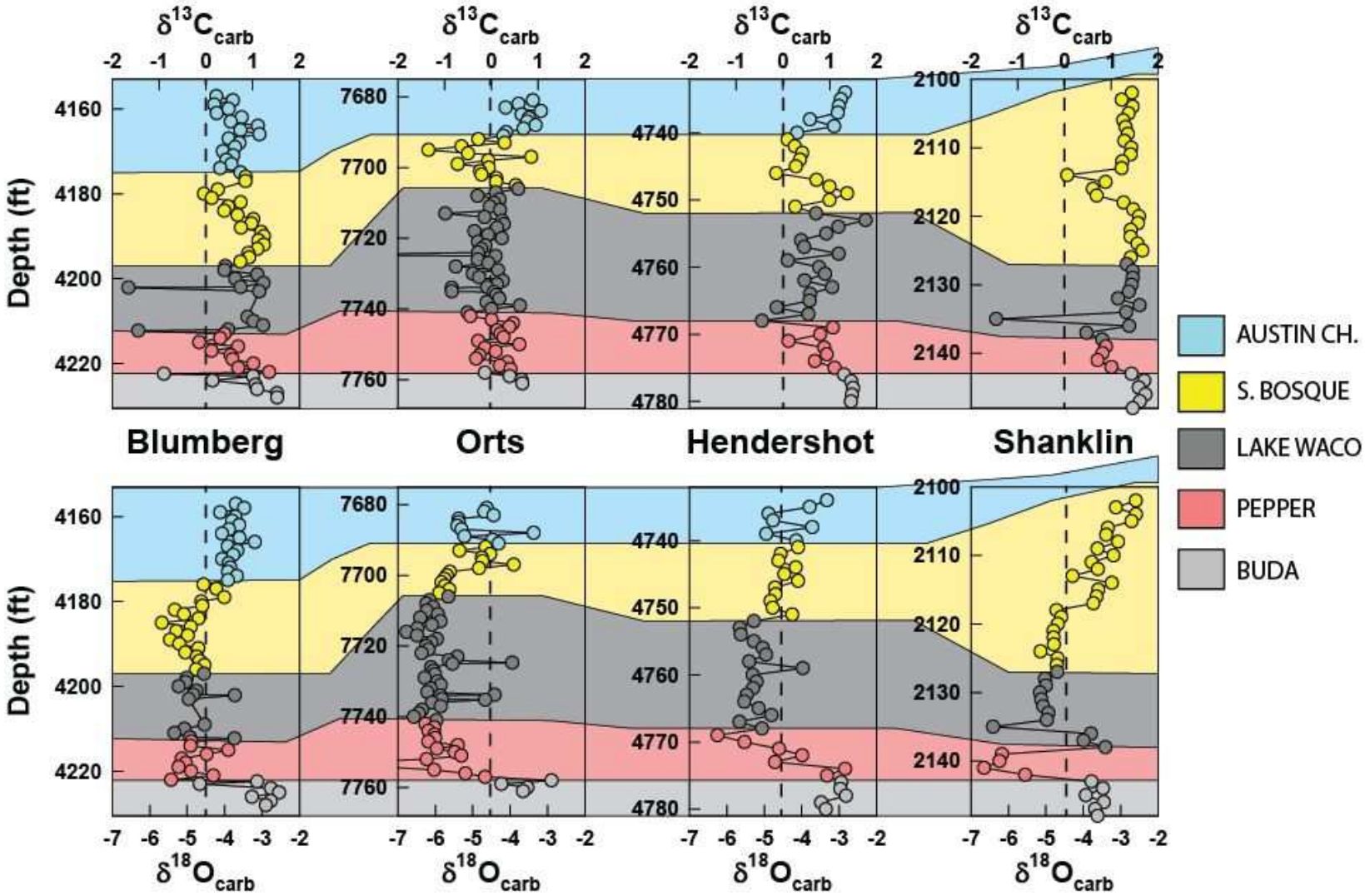

Figure 3.20 δ13C and δ18O versus depth for Blumberg, Orts, Hendershot and Shanklin cores.

Chapter 4

Discussion

4.1 Bulk Geochemistry

4.1.1 Major Elements

Aluminum is often used as a geochemical proxy for clay minerals (i.e. illite). Cross-plots of elements versus aluminum are used to identify what portions of these elements reside in the clay minerals and where these minerals may be enriched or depleted. Enrichment above the clay fraction indicates the element is present in another mineral phase, such as a Si enrichment due to an influx of quartz.

The negative slope displayed in the relationship between Ca and Al (Figure 3.13) indicates the dilution of the clay minerals by calcium carbonate deposition.

Si exhibits a strong linear trend with aluminum (Figure 3.14). There are data points to the left of the trend indicating an enrichment of silicon relative to aluminum. This is an indication that silicon resides in another mineral phase other than clays. This silicon is most likely in the form of quartz. It is not clear whether this excess silicon is biogenic or detrital in nature. This excess is especially evident in the Krause core which displays a Si enrichment in a majority of the samples. This may be an indication of a difference in sediment supply, as this core is located some distance to the west of the other five.

The strong linear trend between Ti and Al (Figure 3.15) suggests that Ti resides predominantly in the clay mineral phase. The deviations that fall above the trend line indicate that titanium is possibly present in another mineral form, potentially rutile (TiO_2).

The cross-plots of K versus Al (Figure 3.16) display a fair amount of variability. Though K-bearing clay mineral illite is the dominant clay mineral, the data points that fall below the trend suggest the presence of other clay minerals that do not contain

potassium. The presence of kaolinite and smectite has been documented along the trend of the Eagle Ford. Kaolinite rich seams have been identified in the Eagle Ford equivalent Boquillas formation of West Texas (Trevino, 1988; Miller, 1990; Lock and Peschier, 2006; Donavan and Staerker, 2010; Ruppel et al., 2012). Numerous ash layers can be found within the Eagle Ford, ranging in size from 0.5 to 6 inches. XRD analysis of these ash layers reveals they consist of approximately 90% clay minerals. Of this clay mineral portion, some ash layers predominately consist of kaolinite (avg. 91%), while others, now in the form of bentonite, have smectite accounting for 80% of the clay portion (Harbor, 2011; Fairbanks, 2012).

Cross-plots of Ca versus Mg (Figure 3.18) display no clear linear trend, aside from the Krause core. This lack of linear trend indicates the possible presence of a Mg bearing carbonate mineral such as ankerite $(Ca(Mg,Fe,Mn)(CO_3)_2$, dolomite $CaMg(CO_3)_2$, or francolite $(Ca, Mg, Sr, Na)_{10}(PO_4, SO_8, CO_2)F_{2-3}$.

Calcite-clay-quartz ternary diagrams were plotted of each for each of the six cores to determine the composition of the Eagle Ford relative to the average marine gray shale, as determined by Wedepohl (1971, 1991). All cores indicate a clay fraction consistent with the average gray shale, but heavily diluted with calcium carbonate. There are instances of minor silica enrichment, but it cannot be determined if this excess silica is detrital or biogenic in origin.

4.2 Paleoceanograpy

4.2.1 Chemical Paleoceanography

Redox sensitive trace metal concentrations in the form of enrichment factors (EFs) were used in Figures 3.1 through 3.6 to evaluate the redox character of the Eagle Ford Group. Enrichment factor values of one indicate levels similar to that of average

gray shale (Wedepohl, 1971, 1991) deposited under normal, oxic conditions. Higher enrichment factors indicate deposition under anoxic or euxinic marine conditions (Calvert and Peterson, 1993; Crusius et al., 1996).

In oxic marine environments, Zn and Ni behave as micronutrients that can be concentrated in organic material (Algeo and Maynard, 2004; Tribovillard, 2006). Upon decay of this organic material these elements are released into the overlying water. However, in euxinic/sulfidic conditions they may be incorporated into pyrite as ZnS and NiS (Tribovillard, 2006). A concentration of these micronutrients is an indication that organic matter was deposited in great abundance and that reducing conditions were present (Tribovillard, 2006).

Molybdenum is generally in the stable, unreactive form of molybdate (MoO_4^{2-}) in normal marine waters with a very long residence time of 800k years and is not readily used in biologic processes (Broeker and Peng, 1982; Algeo and Maynard, 2004). However, under anoxic/euxinic conditions Mo can be readily adsorbed by organic material and transferred to the sediment. Molybdate ions are sequestered to sediments in the presence of sulfide mineral, organic matter, or sulfidized organic matter (Helz et al., 1996).

All six cores indicate enrichment in the redox sensitive trace metals within the Lake Waco and Pepper Shale Formations during what is considered to the reducing, transgressive Lower Eagle Ford. Overlying this, within the South Bosque Formation, these elements are not enriched and contain levels more associated with a more oxygen rich environment.

The stable isotope values represented in Figure 3.20 have proven to be unreliable as a diagnostic tool with which to determine stratigraphy or correlation between

the four cores analyzed. The stratigraphic divisions applied to these are based on the divisions determined by the previously discussed geochemical data.

The general positive excursion of the $\delta^{18}O$ signal seen across all four cores suggests a cooling trend in the South Bosque Formation. Another interpretation of such a trend lies in determining what part of the signal is temperature and what part is affected by salinity changes (Poulson et al., 1999; DeConto et al., 2000). This "salinity effect" is the result of the hydrologic cycle differentiating the $\delta^{18}O$ of the upper layer of the ocean in response to evaporation and precipitation, both of which selectively leave the heavier ^{18}O isotope behind (Poulson et al., 1999; DeConto et al., 2000).

During ocean anoxic events organic carbon accumulates and is preserved due to oxygen depleted conditions in the lower water column. As the lighter ^{12}C is preferred by biologic processes, these OAEs are marked by positive excursions of the $\delta^{13}C$ signal. OAE2, in particular, has shown increases from 1‰-2 ‰ to 4‰-5‰ (Schlanger et al., 1987). None of the four cores analyzed for this study contain such an increase. Based on these $\delta^{13}C$ data, these particular cores do not contain a record of OAE2 at the Cenomanian-Turonian boundary.

4.2.2 Physical Paleoceanography

Hydrographic circulation in marine basins plays an important role in the basin environment and in biogeochemical cycles (Algeo and Rowe, 2011). The degree of restriction of the deep (subpycnoclinal) watermass can be determined by the molybdenum-total organic carbon ratio (Algeo and Lyons, 2006). Figure 4.1 contains the cross-plot of Mo(ppm) concentration versus %TOC for the Krause core along with analogues of other basins that display varying degrees of restriction and deep water renewal. These data suggest intervals of restriction as well as intervals of a more open

environment. This is likely due to the numerous smaller-order transgressive events that occurred during the deposition of the Eagle Ford. In a more restricted basin, with limited water mass renewal, the removal of Mo to the sediment draws down the amount of available Mo. With a lower renewal time, the supply of Mo can be replenished leading to higher values, such as those seen in the Eagle Ford. By comparison, the deep water renewal time of the Saanitch Inlet is <10 yr, while the Black Sea is ~400-800 yr (Algeo and Rowe, 2011). The Lake Waco and Pepper Shale Formations, as represented by the Krause core, were deposited in an environment that was restricted at times, but more open at others, yet remained an anoxoc/euxinic basin.

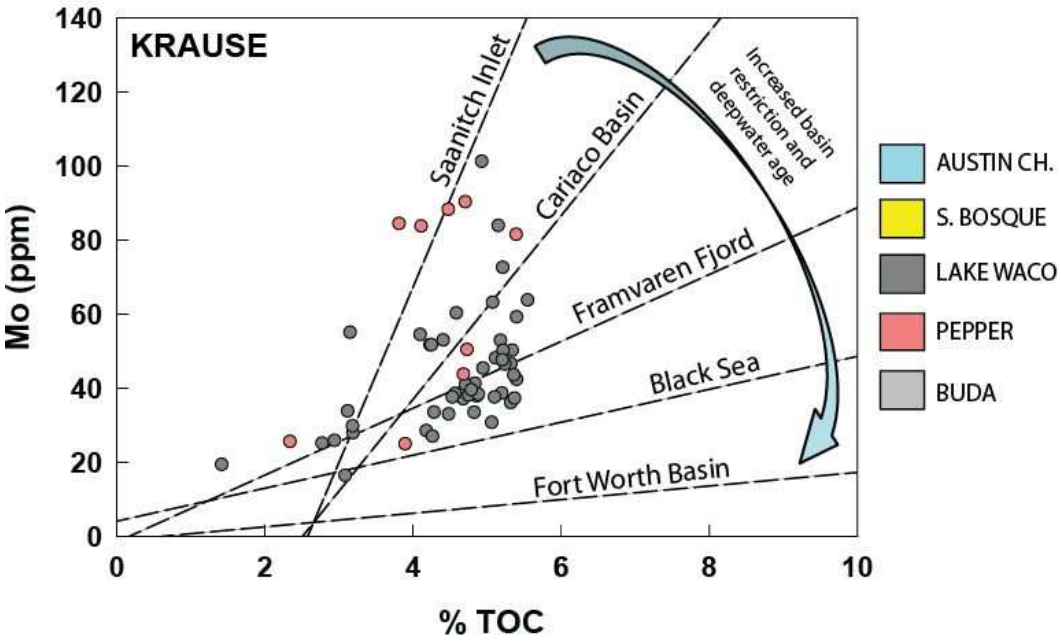

Figure 4.1 Cross-plot of total organic carbon (TOC) versus Mo of A.L. Krause #2 core. Modified after Algeo and Rowe, 2012.

Chapter 5

Conclusions

The utilization of geochemical data has allowed the reconstruction of the paleoceanography and chemostratigraphy of the Cenomanian-Turonian Eagle Ford Group. Elemental concentrations and geochemical proxies have been used to define stratigraphic shifts in mineralogy and paleo-redox conditions of the southwestern end of the Maverick Basin along the Comanche Shelf during what is considered to be the time of OAE2 (~92mya).

Redox sensitive trace metal accumulation was enriched during deposition of the Pepper Shale and Lake Waco Formations due to anoxic or euxinic bottom water conditions. Physical paleoceanographic reconstruction reveals that the Pepper Shale and Lake Waco Formations were deposited during times of restriction and times of more open hydrography, yet anoxic or euxinic conditions remained throughout deposition of these two formations.

The South Bosque Formation is characterized by trace metal concentrations that are more in-line with those of average gray shale, during a time of a more oxygen rich environment.

Numerous studies have shown that the Cenomanian-Turonian boundary and OAE2 are contained with the Eagle Ford Group. Some have place the OAE2 at the top of the South Bosque Formation just below the boundary with the Austin Chalk. Due to the unconformable boundary with the overlying Austin Chalk in this region, and the topographic high created by the San Marcus Arch, it is possible the sediments recording this event were removed prior to Austin Chalk deposition. Others have placed the OAE2 in the upper part of the Lake Waco Formation just below the South Bosque Formation. However, none of the four cores analyzed for this study display the positive excursion of

the $\delta^{13}C_{carb}$ signature associated with this globally correlative event. Due to the topographic high created by the San Marcus Arch, these cores contain a more condensed record of Eagle Ford deposition, as some of the studied cores contain all three formations of the Eagle Ford Group in as little as 40 feet of core, while cores from further out in the Maverick Basin containing the same sequence may be over 600 feet thick. Samples for this study were taken at one foot intervals. It is possible that a higher resolution study, such as sampling at 2 inch intervals, may reveal the presence of OAE2, but it is the determination of this study that this anoxic event in not recorded within the studied cores.

References

Adkins, W.S., and Lozo, E.F., Jr., 1951, Stratigraphy of the Woodbine and Eagle Ford, Waco are, Texas: Southern Methodist University Fondren Science Series, v. 4, p. 105-161.

Algeo, T.J. and Maynard, J.B., 2004. Trace-metal behavior and redox facies in core shales of Upper Pennsylvanian Kansas-type cyclothems. Chemical Geology. 206: 289-318.

Algeo, T.J. and Rowe, H.D. 2011, Paleoceanographic applications of trace-metal concentration data. Chemical Geology. Vol. 324-325, p. 6-18.

Algeo, T.J., and Lyons, T.W., 2006, Mo-total organic carbon covariation in modern anoxic marine environments: implications for analysis of paleoredox and paleohydrographic conditions. Paleoceanography, v. 21, PA1016

Algeo, T.J., Heckel, J.B., Maynard, Blakey, R., Rowe, H., 2008, Modern and ancient epicratonic seas and superestaurine circulation model of marine anoxia, in Holmden and BR Prat, (Eds). Dynamics of Epeiric Seas, Paleontological and Geochemical Perspectives: Geological Association of Canada Special Publication, Vol. 48, p. 7-38.

Aplin, A.C., Fleet, A.J., and Macquaker, J.H.S. 1999. Muds and mudstones: physical and fluid-flow properties. Geological Society, London, Special Publications, v. 158, p. 1-8.

Arthur, M.A., Dean, W.E., and Schlanger, S.O., 1985, Variations in the global carbon cycle during the Cretaceous related to climate, volcanism, and changes in atmospheric CO_2, in Sundquist, E.T., and Broecker, W.S., eds., The Cabon Cycle and Atomospheric CO_2: Natural Variations Archaen to Present, Geophysical Monograph Series. AGU, Washington, D.C., p. 546-553.

Arthur, M.A., Dean, W.E., Pratt, L.M., 1988, Geochemical and climatic effects of increased marine organic carbon burial at the Cenomanian/Turonian boundary: Nature, v. 335, p. 714-717.

Arthur, M.A., Sageman, B.B., 1994. Marine black shales: depositional mechanisms and environments of ancient deposits. Annual Reviews in Earth and Planetary Science. 22: 499–551.

Barron, E.J, 1983. A warm, equable Cretaceous: the nature of the problem. *Earth Sci. Rev*. 19, 305-338.

Blakey, R. 2005. Paleogeography and geologic evolution of North America; images that track the ancient landscapes of North America. Online.

Blatt, H. 1980. Origin of Sedimentary Rocks. Englewood Cliffs, Prentice-Hall. 782 p.

Broecker, W.S., Sutherland, S., Peng, T.H., 1999. A possible 20th century slowdown of southern ocean deep water formation. Science 286, 1132–1135.

Brumsack, H.J., 2006, The trace metal content of recent organic carbon righ sediments: Implications for cretaceous black shale formation, Palaeogeography, Palaeoclimatology, Palaeoecology 232, is. 2-4, p. 344-361.

Calvert, S.E. and Pedersen, T.F. 1993. Geochemistry of recent oxic and anoxic marine sediments: implications for the geological record. Marine Geology. 113: 67–88.

Cherry, M., 2011, A case history of the Eagle Ford oil shale play, South Texas: AAPG Search and Discovery Article #90122, <http://www.searchanddiscovery.com/abstracts/pdf/2011/hedberg-texas/abstracts/ndx_cherry.pdf>

Dawson, W.C., 1997, Shale microfacies: Limestone microfacies and sequence stratigraphy: Eagle Ford Group (Cenomanian-Turonian) north-central Texas outcrops. Gulf Coast Association of Geological Societies Transactions, v. 47, p. 99-105.

Dawson, W.C., 2000. Shale microfacies: Eagle Ford Group (Cenomanian-Turonian) north-central Texas outcrops and subsurface equivalents: Gulf Coast Association of Geological Societies Transactions, v. 50, p. 607-621.

Dean,W.E. and Arthur, M.A. 1989. Iron–sulfur–carbon relationships in organic-carbon-rich sequences I: Cretaceous western interior seaway. American Journal of Science. 289: 708–743.

DeConto, R.M., Olson, B., Suarez, C., Leckie, M., Hay, W., 2000, A reevaluation of Late Cretaceous oceans; comparing ocean climate models and isotopes. 6th International Cretaceous Symposium. Geozentrum, University of Vienna, Vienna, Austria, August 27 to September 4, 2000, 24.

Donovan, A.D., and Staerker, T.S., 2010, Sequence Stratigraphy of the Eagle Ford (Boquillas) Formation in the Subsurface of South Texas and Outcrops of West Texas: Gulf Coast Association of Geological Societies Transactions, v. 60, p. 861-899.

Durham, L.S., 2010, Eagle Ford joins shale elite: AAPG Explorer, http://www.aapg.org/explorer/2010/01jan/eagleford0110.cfm

Engleman, E.E., Jackson, L.L., Norton, D.R. and Fisher, A.G., 1985, Determination of carbonate carbon in geological materials by coulometric titration. Chemical Geology. 53: 125-128.

Haq, B.U., Hardenbol, J., Vail, P.R., 1986, Chronology of fluctuating sea levels since the Triassic (250 million years ago to present), Science, v. 235, p. 1156-1167.

Harbor, R.L., 2011, Facies Characterization and Stratigraphic Architecture of Organic-Rich Mudrocks, Upper Cretaceous Eagle Ford Formation: MS thesis, University of Texas at Austin. 184 p.

Harrison, C.G.A., 1990. Long-term eustasy and epeirogeny in continents. In: Revelle, R. (Ed.), Sea Level Change. U.S. National Academy Press, Washington, D.C., pp. 141–158.

Hetzel, A., Bottcher, M.E., Wortmann, U.G., Brumsack, H.J., Paleo-redox conditions during OAE2 reflected in Demerara Rise sediment geochemistry (ODP Leg 2070, Palaeogeography, Palaeoclimatology, Palaeoecology, v. 273, p. 302-328.

Hill, R.T., 1901, Geography and geology of the Black and Grand Prairies, Texas: USGS 21st Annual Report, pt. 7, 666 p.

Jenkyns, H.C., 2010, Geochemistry of oceanic anoxic events, Geochemistry, Geophysics, Geosystems, v. 11 p. 1-30.

Kauffman, E.G., 1984, Paleobiogeography and Evolutionary Response Dynamic in the Cretaceous Western Interior Seaway of North America. Geological Association of Canada Special Paper, 27

Kolonic, S., Wagner, T., Forester,A., Sinninghe Damste, J.S., Walsworth-Bell, B., Erba, E., Turgeon, S., Brumsack, H.J., Chellai, E.H., Tsikso, H., Kuhnt, W., Kuypers, M.M.M.,2005, Black shale deposition on the northwest African shelf during the Cenomanian/Turonian oceanic anoxic event: Climate coupling and global organi carbon burial. Paleoceanography, v.20.

Kuypers, M.M.M., Blokker, P., Erbacher, J., Kinkel, H., Pancost, R.D., Schouten, S., Sinninghe Damste, J.S., 2001. Massive Expansion of Marine Archaea During a Mid-Cretaceous Oceanic Anoxic Event. Science, v. 293, p. 92-94.

Lock, B.E., Bases, F.S., and Glaser, R.A., 2007, The Cenomanian sequence stratigraphy of Central to West Texas: Gulf Coast Association of Geological Societies Transactions, v. 57, p. 465-479.

Lock, B.E., Pechier, L., 2006, Boquillas (Eagle Ford) Upper Slope Sediements, West Texas: Out crop Analogs for Potential Shale Reservoirs, GCAGS Annual Convention, AAPG Search and Discovery article #90056

Mancini, E. A., and Puckett, M., 2005, Jurassic and Cretaceous Transgressive-Regressive (T-R) Cycles, Nothern Gulf of Mexico, USA. Stratigraphy, Vol.2, No. 1, 31-48.

Pessagno, E.A., 1969, Upper Cretaceous stratigraphy of the western Gulf Coast area of Mexico, Texas and Arkansas: Geological Society of America Memoir 111, 139 p.

Piper, D.Z. 1994. Seawater as the source of minor elements in black shales, phosphorites and other sedimentary rocks. Chemical Geology. 114: 95-114.

Piper, D.Z. and Calvert, S.E. 2009. A marine biogeochemical perspective on black shale deposition. Earth-Science Reviews. 95: 63-96.

Piper, D.Z., Perkins, R.B., 2004, A modern vs. Permian black shale-the hydrography, primary productivity, and water-column chemistry of deposition, Chemical Geology, v. 206, is. 3-4, p. 177-197.

Potter, P. E., Maynard, J.B. and Pryor, W.A. 1980. Sedimentology of Shale: New York, Springer Verlag. 306 p.

Poulsen, C.J., Gendaszek, A.S., Jacob, R.L., 2003. Did the rifting of the Atlantic Ocean cause the Cretaceous thermal maximum. Geology 31, 115–118.

Prather, J.K., 1902, A preliminary report on the Austin Chalk underlying Waco, Texas, and the adjoining territory: Texas Academy of Science, Transactions, v. 4, p. 115-122.

Railroad Commission of Texas, 2014, Eagle Ford Information, http://www.rrc.state.tx.us/eagleford/index.php#general

Rimmer, S.M. 2004. Geochemical paleoredox indicators in Devonian-Mississippian black shales, Central Appalachian Basin (USA). Chemical Geology. 206: 373-391.

Rousseau, R.M., 2001, Detection limit and estimate of uncertainty of analytical XRF results: The Rigaku Journal, v. 18, p. 33-47.

Rowe, H., Hughes, N., Robinson, K., 2012. The quantification and application of handheld energy-dispersive x-ray fluorescence (ED-XRF) in mudrock chemostratigraphy and geochemistry, Chemical Geology, 324-325, 122-131.

Rowe, H.D. and Hughes, N., 2010, Strategy for Developing and Calibrating Shale and Mudstone Chemostratigraphies Using Hand-Held X-Ray Fluorescence Units, AAPG Annual Convention, Unmasking the Potential of Exploration and Production. Search and Discovery Article #90104.

Rowe, H.D., Loucks, R.G., Ruppel, S., Rimmer, S.M., 2008, Mississippian Barnett Formation, Fort Worth Basin, Texas: Bulk geochemical inferences and Mo-TOC constraints on the severity of hydrographic restriction: Chemical Geology v. 257, p. 16-25.

Sahagian, D., Pinous, O., Olferiev, A., Zakaharov, V., Beisel, A., 1996, Eustatic curve for the Middle Jurassic-Cretaceous based on Russian platform and Siberian stratigraphy: Zonal resolution, American Association of Petroleum Geologists Bulletin 80, p. 1433-1458.

Schieber, J., and Zimmerle, W. 1998. Introduction and overview: The history and promise of shale research, in J. Schieber, W. Zimmerle, and P. Sethi, eds., Shales and Mudstones I: Stuttgart, Germany, E. Schweizerhbart'sche Verlagsbuchhandlung, p. 1-10.

Sellards, E.H., Adkins,W.S., Plummer, F.B., 1932, The geology of Texas,I: Stratigraphy: The University of Texas Bulletin No. 3232, p 422-439.

Sinton, C.W., and Duncan, R.A., 1997, Potential links between ocean plateau volcanism and global anoxia at the Cenomanian-Turonian boundary: Economic Geology, v. 92, p. 863-842.

Udden, J.A., 1907, A sketch of the geology of the Chisos country, Brewster County, Texas: University of Texas Bulletin 93, Austin, p. 29-33.

Vail, P.R., Mitchum Jr., R.M., Thompson III, S., 1977. Global cycles of relative changes of sea level. In: Payton, C.E. (Ed.), Seismic Stratigraphy and Global Changes of Sea Level. American Association of Petroleum Geologists Memoir 26, 83–97

Verardo, D.J., Froelich, P.N., and McIntyre, A., 1990, Determination of organic carbon and nitrogen in marine sediments using the Carlo Erba NA-1500. Deep-Sea Research, 37: 157-165.

Wignall, P.B., 1994, Black Shales: Geology and Geophysics Monographs, 30. Oxford, Oxford University Press, 130p.

Williams, G.D., and Stelck, C.R., 1975, Speculations on the Cretaceous Palaeogeography of North America: in Caldwell, W.G.E., eds.. The Cretaceous System in the Western Interior of North America: Geological Association of Canada Special Paper 13, p. 1-20.

Young, K., 1977, Guidebook to the Geology of Travis County, in Jones, E., ed., 2011: The University of Texas at Austin, Austin, TX. http://www.lib.utexas.edu/geo/ggtc/toc/html.

Biographical Information

Robert Francis Nikirk was born on October 5, 1971 in Forth Worth, Texas. Robert grew up in Alvord, Texas and graduated from Alvord High School in 1990 as valedictorian of his class. He then attended the University of Texas at Arlington in pursuit of a degree in Business Administration. After years of labor in the business industry, he returned to full-time university studies at the University of Texas at Arlington in 2008. Robert earned a Bachelor of Science degree in Geology in 2011. He then entered the Master of Science program at the University of Texas at Arlington under the supervision of Dr. Harry Rowe. He is scheduled to complete his Master of Science degree in Geology in May 2014.